MT-CWR-094-038

FINAL REPORT

JOINT INDUSTRY UNDERWATER WELDING CONSUMABLES DEVELOPMENT PROGRAM (CSM ACTIVITIES)

Submitted by:
Stephen Liu, David L. Olson and Charles Johnson
Center for Welding and Joining Research
Colorado School of Mines
Golden, Colorado 80401

Submitted to:
JIP - Technical Activities Committee
Attn: Mr. C. E. Grubbs
Global Divers, Inc.
Lafayette, Louisiana

November 1994

CSM

CENTER FOR WELDING AND JOINING RESEARCH
Colorado School of Mines
Golden, Colorado 80401

MT-CWR-094-038

FINAL REPORT

JOINT INDUSTRY
UNDERWATER WELDING CONSUMABLES DEVELOPMENT PROGRAM
(CSM ACTIVITIES)

Submitted by:

Stephen Liu, David L. Olson and Charles Johnson

Center for Welding and Joining Research

Colorado School of Mines

Golden, Colorado 80401

Submitted to:

JIP - Technical Activities Committee

Attn: Mr. C. E. Grubbs

Global Divers, Inc.

Lafayette, Louisiana

November 1994

TABLE OF CONTENTS:

1. BACKGROUND

One of the objectives of the Joint Industry Underwater Welding Development Program (JIP) is to formulate wet welding consumables that exhibit good welding performance and produce welds of acceptable quality. More specifically, the task undertaken by the Center for Welding and Joining Research of the Colorado School of Mines targets the screening of multiple flux systems and the selection of one flux formulation for the JIP. A total of twelve flux coating compositions were designed for testing on two core rods. The fluxes were dry mixed at the Colorado School of Mines (CSM) and extruded by J.M. Minerals, Inc. in Darby, Philadelphia. The experimental electrodes were then used to perform multiple pass welds by Global Divers, Inc. at -33 ft. deep water. Bend testing, hardness measurements, chemical analysis, and X-ray radiography were performed on all twenty four experimental welds to screen the electrodes. Out of these welds, four were selected for further and more thorough characterization, which included the determination of impact toughness and tensile properties, and microstructural characterization. Based on these results, one flux composition was identified and recommended to the JIP.

As a result of the programmed additions of $CaCO_3$, ZrO_2, and Fe-Mn to the flux coating, several experimental electrodes performed exceptionally. In terms of porosity, 10 out of the 24 welds met AWS D3.6 Class A (dry) weld classification, while 12 welds met the requirements for Class B (wet) welds. In terms of Charpy-V-notch impact testing, all four welds passed and exceeded the AWS D3.6 Specification requirement of 15 ft-lbs (20J) at 32°F (0°C). Careful analysis of the weld data led to a better understanding of the interaction between flux ingredients and weld properties, such as weld metal composition, porosity and electrode weldability.

2. EXPERIMENTAL PROCEDURE

All welds were made on 5/8 or 3/4 in. thick, V-grooved ASTM 537 or ASTM A36 steel plates as specified by the TAC members. Experimental electrodes developed by CSM researchers and extruded by J.M. Minerals, Inc. were used to perform these welds in the facilities of Global Divers, Inc., at -33 ft. water depth.

2.1 Electrode Formulation and Electrode Extrusion

The flux coating composition text matrix was developed based on chemical analysis and X-ray analysis results of a prior experimental electrode - Ex7. This electrode was proposed

by Global Divers, Inc. after a thorough evaluation of several commercial electrodes commonly used for underwater wet welding. To duplicate the program experimental electrode, to improve its performance and weld quality, and to increase the toughness of the ferritic weld metal matrix such that it can tolerate the presence of some porosity in the weld metal, alloy and flux additions to the Ex7 electrode coating were proposed by CSM-CWJR researchers.

It has been reported in the literature that underwater wet welds generally suffer significant losses of hardenability elements because of oxygen pickup. As such, manganese must be replenished in the weld metal to regain its hardenability. The increase of manganese content in the weld system would also improve the degree of deoxidation of the weld pool. The amount of ferro-manganese additions ranged from 8 to 14 wt. pct.

During decomposition, calcium carbonate generates CO_2 which decreases the partial pressure of H_2 in the arc. As a result of the hydrogen decrease, weld metal porosity is expected to reduce accordingly. Therefore, two levels of $CaCO_3$, 3.2 and 6.2 wt. pct., were added to the otherwise E6013 type electrode coating. Additionally, 5 to 8 wt. pct. of ZrO_2 were also added to the flux coating to yield a test matrix of twelve flux compositions. The composition of the experimental fluxes are shown in Table I. Notice that the addition of $CaCO_3$, ZrO_2, and Fe-Mn modified profoundly the nature of the welding slag, no longer an E6013 type, and its reactivity with the weld puddle resulted in modified weld metal chemical composition and microstructure.

To expedite the electrode manufacturing process, the JIP-TAC decided best to utilize J.M. Minerals, Inc. for the extrusion process. Industrial grade chemicals according to the flux formulations were weighed and blended at CSM. The dry mixes were then shipped to J.M. Minerals, Inc. for further processing with the potassium silicate binder. Small amounts of hydroxide and siliceous material, and CMC (Cellulose Methyl Carbonyl) were also added as extrusion agent. J.M. Minerals, Inc. was also responsible for the acquisition of the low carbon steel and ultra-low carbon steel core rods used. The core rods were 1/8 in. diameter and 14 in. length. The chemical composition of the core rods are shown in Table II.

2.2 Welding Parameters and Joint Design

The welding parameters used in producing the experimental welds were determined by Global Divers, Inc. and are reported in the following. For the low carbon steel welding electrodes, the welding current varied between 145 and 170 amperes, and the voltage, from 25 to

Table I. Chemical composition (in wt. pct.) of the flux systems developed in this research program.

	J-1	J-2	J-3	J-4	J-5	J-6	J-7	J-8	J-9	J-10	J-11	J-12
TiO_2	54.5	47.5	51.5	51.5	44.5	44.5	50.5	51.5	47.5	48.5	45.5	42.5
SiO_2	4.4	4.4	4.4	4.4	4.4	4.4	4.4	4.4	4.4	4.4	4.4	4.4
Fe ①	1.5	1.5	1.5	1.5	1.5	1.5	1.5	1.5	1.5	1.5	1.5	1.5
Feldspar ②	7	7	7	7	7	7	7	7	7	7	7	7
Kaolin	2.6	2.6	2.6	2.6	2.6	2.6	2.6	2.6	2.6	2.6	2.6	2.6
Mica	4.5	4.5	4.5	4.5	4.5	4.5	4.5	4.5	4.5	4.5	4.5	4.5
$CaCO_3$	3.2	3.2	6.2	6.2	6.2	6.2	3.2	3.2	6.2	6.2	3.2	6.2
ZrO_2	5	8	5	5	8	8	5	8	5	8	8	8
Fe-Mn	8	12	8	8/10	8/10	12	12	8	12	8	14	14
KPS	9.3	9.3	9.3	9.3	9.3	9.3	9.3	9.3	9.3	9.3	9.3	9.3

① Reduced Iron Powder
② Sodium Feldspar

Table II. Chemical composition (in wt. pct.) of the low carbon steel and ultra-low carbon steel core rods used in extrusion.

Core Rod	C	Mn	P	S	Si	Ni	Cr	Cu
Low carbon steel	0.069	0.63	0.008	0.016	0.08	0.03	0.02	0.03
Ultra-low carbon steel	0.019 max	--	--	--	--	--	--	--

35 volts. The travel speed was between 7.9 and 14.6 ipm. For the ultra-low carbon steel electrodes, the ranges of welding current and voltage were much narrower, from 150 to 160 amperes, and from 25 to 30 volts, respectively. The travel speed for these electrodes varied from 6.0 to 15.5 ipm. The individual welding data are given in Tables III and IV.

2.3 X-Ray Radiography

All weld specimens were inspected by X-ray radiography for defects such as porosity and entrapped slags. Furthermore, the welds were classified according to the criteria established in

Table III. Welding parameters used in the experimental welds with the low carbon steel electrodes.

Electrode	Weld	Passes	Amperes	Volts	ipm
LC-1 ①	Root	2	150	32	7.9
	Fill and Cap	24	155	35	11.7
LC-2 ①	Root	2	145	25	8.7
	Fill and Cap	25	160	30	9.8
LC-3 ①	Root	2	150	25	8.6
	Fill and Cap	25	165	30	10.4
LC-4 ①	Root	2	155	28	9.0
	Fill and Cap	24	155	28	10.7
LC-5 ②	Root	2	155	25	8.4
	Fill and Cap	35	155	25	13.0
LC-6 ②	Root	2	155	25	8.2
	Fill and Cap	35	155	25	14.6
LC-7 ③	Root	1	150	26-28	6.7
	Fill and Cap	42	150	26-28	12-16
LC-8 ③	Root	1	160	30	5.2
	Fill and Cap	41	160-170	33-35	11-16
LC-9 ③	Root	1	160	30	6.6
	Fill and Cap	43	160	30	12-16
LC-10 ③	Root	1	160	28	5.1
	Fill and Cap	46	160	28-30	12-16
LC-11 ③	Root	1	160-165	30	5.7
	Fill and Cap	41	150-170	28-30	15-16
LC-12 ③	Root	1	150	25-30	7.2
	Fill and Cap	39	160	30-35	13-15

① 5/8 x 10 in. Vertical Groove Welds - A537 Steel
② 3/4 x 14.5 in. Vertical Groove Welds - A537 Steel
③ 3/4 x 14.5 in. Vertical Groove Welds - A36 Steel

the AWS D3.6 Specification. The radiographic films and their interpretation were provided to CSM by Global Divers, Inc.

2.4 Metallographic Characterization

To characterize the microstructure of four sets of experimental welds, a light metallograph was used. Polished and etched transverse cross-sections of the welds were examined at the magnifications of 200 and 500X. A nital (2 vol. pct.) solution was used to etch the specimens to reveal the microstructure. Quantitative metallography work using an image analyzer was carried out to determine the volume fractions of acicular ferrite, grain boundary ferrite and FS phases.

Table IV. Welding parameters used in the experimental welds with the ultra-low carbon steel electrodes.

Electrode	Weld	Passes	Amperes	Volts	ipm
UL-1 ①	Root	2	160	26	9.3
	Fill and Cap	36	160	26	10.6
UL-2 ①	Root	2	155	30	10.6
	Fill and Cap	34	150	25	11.3
UL-3 ①	Root	2	150	26	9.3
	Fill and Cap	35	155	27	11.5
UL-4 ①	Root	2	150	27	8.0
	Fill and Cap	38	165	26	11.1
UL-5 ①	Root	2	160	27	6.0
	Fill and Cap	34	158	26	11.0
UL-6 ①	Root	2	160	28	7.0
	Fill and Cap	34	160	28	10.6
UL-7 ②	Root	1	160	30	7.5
	Fill and Cap	41	160	30	14.9
UL-8 ②	Root	1	160	30	7.5
	Fill and Cap	33 ③	160	30	11.5
UL-9 ②	Root	1	160	30	7.2
	Fill and Cap	43	160	30	13.4
UL-10 ②	Root	1	160	30	7.3
	Fill and Cap	40	160	30	14.6
UL-11 ②	Root	1	160	30	6.8
	Fill and Cap	41	160	30	15.5
UL-12 ②	Root	1	160	30	7.6
	Fill and Cap	42	160	30	14.9

① 3/4 x 14.5 in. Vertical Groove Welds - A36 Steel
② 3/4 x 14.5 in. Vertical Groove Welds - A36 Steel
③ Weld was not completed.

Visual inspection of the capping passes with respect to tie-in, ripple pattern, fine cracking, undercut, and spatter was also conducted.

2.5 Chemical Analysis

Chemical analysis of all welds were performed using an emission optical spectrometer. In particular, the carbon, sulfur, oxygen, and nitrogen contents of the welds were determined using interstitial analyzers.

2.6 Mechanical Testing

Bend tests and hardness measurements were conducted on all twenty four experimental welds to screen the electrodes. Since the thickness of the weld plates used were greater than 3/8 in., side bends were preferred. The method of bend testing with progressive ~~increase~~ decrease in radius of bend curvature, as described in the previous JIP Interim Reports, was adopted in these tests. The procedure consists of bending a specimen at 6T. If no cracks are detected, the test then proceeds to 4T, 3-1/3T, and finally 2T. Each step is followed by careful inspection for the presence of cracks. If a specimen fails at any intermediate radius, the test is discontinued and the result recorded.

The hardness of the different weld zones were measured using a Vickers hardness tester with 1 kg load. Because of the importance of surface preparation to the accuracy and repeatability of the hardness readings, the weld specimens were polished and lightly etched with a 2 vol. pct. Nital solution.

Four welds were selected from the 24 weld sets for further and more thorough characterization, which included the determination of impact toughness, tensile properties and microstructure. Charpy-V-notch impact tests were carried out using full-sized specimens (10 x 10 x 50 mm) at 28°F. The amount of energy absorbed at fracture, fracture appearance (percent ductile shear), and lateral expansion of the specimen were recorded and compared with the AWS D3.6 Specification requirements. ~~Reduced-section~~ All-weld-metal tensile specimens were used to determine the yield and tensile strengths, elongation, and reduction in area of the welds. More detailed information on the geometry of the test specimens and testing procedure can be found in the ANSI/AWS B4.0 - Standard Methods for Mechanical Testing of Welds.

3. RESULTS AND DISCUSSION

3.1 Electrode Extrusion

As explained in the Experimental Procedure Section, the electrodes were extruded by J.M. Minerals, Inc. In Darby, Philadelphia. A die size of 0.214 in. was used with varied extrusion pressure, which ranged between 2000 and 6000 psi. The large variation in die pressure resulted because of the different ingredients added to the fluxes. The core rods were all well centered with respect to the flux coating. According to the "scribe" test results, a small number of lines marked

on the wet flux coating, while rotating the electrode in a jig with a series of tools at fixed distances from the center of the rod, indicates better concentricity of the core rod. Up to 10 lines are admissible in a production environment. Based on this criterion, the experimental electrodes showed minimum eccentricity, with only a small scatter of two to seven lines.

The final diameter of the electrodes varied between 0.208 and 0.217 in. With a core rod diameter of 0.125 in., the flux coating thickness varied between 0.0415 and 0.0460 in. Comparison with the Global program electrode - Ex7 - which has a coating thickness of 0.0439 in., shows that the experimental electrodes matched very favorably with the commercial electrodes. Table V shows some of the processing data obtained from J.M. Minerals, Inc. with respect to the extrusion behavior of the electrodes.

Table V. Typical extrusion data of some of the experimental fluxes.

Flux System	Extrusion Pressure (psi)	Concentricity (No. of lines)	Final Diameter (Middle Section) (in.)
LC-1	5000	3	0.212
LC-2	5000	4	0.209
LC-3	6500	4	0.209
LC-4	8000	2	0.211
LC-5	3500	3	0.209

3.2 Electrode Weldability

The experimental electrodes were tested by Global Divers, Inc. and the performance of the individual batches of electrodes are reported below in Tables VI and VII. According to the results presented in the Global test reports, and in addition to the specific information provided in the tables below, all electrodes had very good arc start/restart characteristics and produced adequate to generous amounts of molten slag. Some of the electrodes produced more fluid slags which required higher travel speed for welding control. With higher alloying content, the electrodes produced more slag than the Ex7 electrode.

Visual inspection of the welds revealed good to excellent bead surface, with smooth ripple pattern and tie-ins. In most of the welds, undercutting and spatter were at a minimum.

Specifically referring to electrode performance, the best flux system was LC-3. However, the best electrode must combine good weld metal properties with reliable electrode performance. Thus, the electrode performance data presented in Tables VI and VII must be used in conjunction with other weld properties for the selection of the target electrode.

Table VI. Performance of the low carbon experimental welding electrodes. (Global Evaluation)

Electrode	Electrode Performance
LC-1	Weldability, flux burn-off, and slag behavior varied from rod to rod.
LC-2	Arc wandered due to uneven flux burn-off. Slag coverage excessive but controllable.
LC-3	Electrode performed well. Slag was easily removed.
LC-4	Good weldability and bead contour. Penetration appeared to be good.
LC-5	Easy arc start. Smooth stable arc. Good weldability.
LC-6	Slag coverage excessive but controllable. Arc starts and restarts were excellent. Very good stop craters with no porosity.
LC-7	Arc tends to wander due to long arc length. Slow flux burn-off contributed to "toe-nailing".
LC-8	Flux coating was uneven on some electrodes. Surface porosity in cap passes.
LC-9	Electrode performance was good.
LC-10	Electrode performance was good.
LC-11	Electrode performacne was good.
LC-12	Electrode performacne was good.

Table VII. Performance of the ultra-low carbon experimental welding electrodes. (Global Evaluation)

Electrode	Electrode Performance
UL-1	In spite of corrective efforts, stop craters had pockets of porosity. Some surface porosity.
UL-2	Smooth stable arc. Moderate deposition. Slag easily removed.
UL-3	Amperage fluctuated 10 to 15 amperes. Long arc length. Very hot arc starts.
UL-4	Smooth stable arc. Slag very fluid. Solidified slag easily removed.
UL-5	Slag excessive and granular. Good, porosity free, top craters.
UL-6	Slag excessive and granular. Stop craters Okay.
UL-7	Electrode performance was fair to good.
UL-8	Midway into fill passes, porosity began to develop and as it worsened the weld was discontinued.
UL-9	Same porosity problem as with UL-8, but with grinding between weld layers, weld was completed.
UL-10	Welded very good until last layer of cap passes. Had some surface porosity.
UL-11	Had to grind surface porosity in fill passes before depositing cap passes.
UL-12	Had to grind surface of fill passes before depositing cap passes.

3.3 Chemical Composition of Welds

The chemical composition of the welds were determined and listed in Table VIII. As expected, the welds contained low sulfur and phosphorus content. Nitrogen content also appeared to be normal, between 70 and 100 ppm. Only one weld showed a slighlty higher nitrogen content. At the levels indicated in Table VIII, these elements do not seem to affect the properties of the welds. Carbon, manganese, silicon, and oxygen are the four elemens that varied significantly with the programmed flux additions. These elements would also be responsible for microstructural and property changes in a weld metal. For the $CaCO_3$, ZrO_2 and Fe-Mn additions made in this experimental program, welds made with the low carbon steel core rod electrodes showed carbon variations between 0.134 and 0.065 wt. pct. Manganese varied between 0.81 and

Table VIII. Chemical composition (in wt. pct.) of the low carbon and ultra-low carbon electrode welds. (Oxygen and nitrogen in ppm)

Weld	C	S	P	N	O	Mn	Si
LC-1	0.071	0.017	0.012	90	1600	0.45	0.42
LC-2	0.085	0.014	0.020	140	1040	0.69	0.31
LC-3	0.065	0.017	0.019	50	1010	0.43	0.41
LC-4	0.094	0.014	0.010	100	1630	0.48	0.42
LC-5	0.076	0.014	0.023	70	990	0.58	0.40
LC-6	0.103	0.017	0.020	70	1190	0.62	0.28
LC-7	0.072	0.014	0.013	110	920	0.59	0.46
LC-8	0.065	0.018	0.019	90	1030	0.41	0.50
LC-9	0.075	0.015	0.025	90	870	0.61	0.36
LC-10	0.074	0.018	0.017	90	850	0.45	0.41
LC-11	0.134	0.014	0.020	70	1550	0.81	0.53
LC-12	0.093	0.018	0.028	100	850	0.69	0.39
UL-1	0.085	0.016	0.012	60	1610	0.55	0.70
UL-2	0.061	0.014	0.021	90	900	0.68	0.50
UL-3	0.061	0.016	0.014	90	950	0.42	0.36
UL-4	0.068	0.017	0.012	80	1630	0.48	0.35
UL-5	0.068	0.015	0.021	100	1350	0.59	0.34
UL-6	0.082	0.018	0.016	110	1240	0.63	0.26
UL-7	0.062	0.022	0.016	90	860	0.64	0.47
UL-8	0.067	0.018	0.013	90	820	0.49	0.48
UL-9	0.066	0.018	0.019	90	990	0.54	0.36
UL-10	0.065	0.021	0.013	90	1070	0.40	0.46
UL-11	0.079	0.017	0.021	90	1070	0.75	0.50
UL-12	0.127	0.019	0.021	196	1257	0.70	0.41

0.41 wt. pct. Silicon also experienced substantial variations, from 0.53 to 0.28 wt. pct. Oxygen variation was equally important, from 850 to 1610 ppm. Notice that the concentrations reported here include contributions from the elements in both "combined" (as inclusions) and "free" (as solid-solution) form. For example, the silicon readings will include both silicon and silicates. The effect of chemical composition will be discussed in a Section 3.8.

3.4 Radiographic Analysis

Excellent results were obtained with respect to porosity control in the experimental welds. Several of the electrodes produced welds that classified AWS D3.6 Class A (Dry) welds. The level of porosity resulted from the remaining electrodes were at least comparable to the welds made with the program electrode, Ex-7. The amount of porosity observed in the present welds, as indicated in Table IX, was based on comparison with a 3G groove weld prepared using Ex-7 electrodes at -33 ft. water depth. Eleven of the twenty four welds exhibited less porosity than the Ex7 weld.

3.5 Bend Test

To determine the effect of the flux additions, the quality of the experimental welds were determined using side bend tests. For Class A welds, AWS D3.6 Specification requires bending radii from 2T to 3-1/3T, depending on the minimum specified base metal yield strength. For wet welds, the specification requires only 6T bending. The bend tests in this program followed a procedure demonstrated previously by Global Divers, Inc. The bending of each specimen started on a 6T mandrel and progressed to 4T, 3-1/3T, and 2T, or to failure. The results of these 24 tests are shown in Table X. With the exception of UL-8 and UL-10, all the remaining welds (22 out of 24) met the wet weld specification of successful 6T bending. In fact, 22 welds passed 4T bending, 18 qualified 3-1/3T bending, and two welds tested 2T bending successfully. Most specimens failed at locations near the center of the weld metal. Some welds showed additional cracks along the heat affected zone/fusion line region.

3.6 Hardness Testing

Hardness measurements were made on the transverse cross-sections of all 24 welds, using the Vickers 1 kg scale. In general, a minimum of 27 hardness readings were made on each weld specimen: 15 in the weld metal and 12 in the heat affected zone. For the low carbon steel electrode welds, the hardness readings varied between 160 and 319 HV-1 for the weld metal, and

Table IX. Weld porosity and classification according to AWS D3.6 Specification.

Weld	Acceptability	Porosity	Weld	Acceptability	Porosity
LC-1	Class B	More	UL-1	Class B	More
LC-2	Class A	Less	UL-2	Class B	More
LC-3	Class B	More	UL-3	Class B	More
LC-4	Class B	More	UL-4	①	More
LC-5	Class B	More	UL-5	Class A ②	Less
LC-6	Class B	Less	UL-6	Class A	Less
LC-7	Class A	Less	UL-7	Class A	Less
LC-8	Class B	More	UL-8	③	More
LC-9	Class A	Less	UL-9	Class B	More
LC-10	Class B	More	UL-10	Class B	More
LC-11	Class A	Less	UL-11	Class A	Less
LC-12	Class A	Less	UL-12	Class A	Less

① Excessive porosity of diameter > 1/16 in. ② Lack of fusion unrelated to electrode performance.
③ Incomplete weld due to excessive porosity.

Table X. Side bend test results of the twenty four experimental welds.
[(+) Weld metal meets specification; (-) Weld metal fails to meet specification.]

Weld	6T	4T	3 1/3T	2T	Weld	6T	4T	3 1/3T	2T
LC-1	+	+	+	-	UL-1	+	+	-	
	+	+	-			+	+	-	
LC-2	+	+	-		UL-2	+	+	+	-
	+	+	+	-		+	+	+	-
LC-3	+	+	-		UL-3	+	+	+	-
	+	+	-			+	+	+	-
LC-4	+	+	-	-	UL-4	+	+	+	-
	+	+	+	+		+	+	-	
LC-5	+	+	+	-	UL-5	+	+	+	-
	+	+	+	+		+	+	+	-
LC-6	+	-			UL-6	+	+	-	
	+	+	+	-		+	+	+	-
LC-7	+	+	-		UL-7	+	+	+	-
	+	-				+	+	+	-
LC-8	+	-			UL-8	-			
	+	-				-			
LC-9	+	+	+	-	UL-9	+	+	+	-
	+	+	+	-		+	+	+	-
LC-10	+	+	+	-	UL-10	-			
	+	+	+	-		-			
LC-11	+	+	+	-	UL-11	+	+	+	-
	+	+	+	-		+	+	+	-
LC-12	+	+	+	-	UL-12	+	+	+	-
	+	-				+	+	+	-

between 200 and 492 HV-1 for the heat affected zone. For the ultra-low carbon steel electrode welds, the hardness distribution was 146 to 312 HV-1 (weld metal) and 200 to 446 HV-1 (heat affected zone). Notice the relatively large variation in the heat affected zone hardness, result of hardness reading from two base plates, ASTM A537 and ASTM A36 steel. Figure 1 shows some sample hardness readings and the locations where typical hardness measurements were taken in this research work. The average hardness readings are summarized in Table XI. The remaining hardness data are included in Appendix I.

Table XI. Average weld metal and heat affected zone hardness readings of the experimental welds.

Weld	Average Weld Metal Hardness (HV-1)	Average Heat Affected Zone Hardness (HV-1)	Weld	Average Weld Metal Hardness (HV-1)	Average Heat Affected Zone Hardness (HV-1)
LC-1	209	262	UL-1	202	289
LC-2	214	311	UL-2	237	265
LC-3	195	303	UL-3	204	263
LC-4	203	302	UL-4	186	254
LC-5	216	243	UL-5	222	294
LC-6	179	251	UL-6	222	251
LC-7	220	249	UL-7	197	253
LC-8	185	283	UL-8	201	338
LC-9	219	277	UL-9	201	274
LC-10	209	271	UL-10	199	296
LC-11	240	244	UL-11	234	301
LC-12	250	263	UL-12	210	255

3.7 Complete Weld Qualification for Four Selected Weldments

Based on the results obtained in the six previous tasks (Section 3.1 to 3.6), four weldments were selected for further characterization, which included the determination of tensile properties (σ_y - yield strength, σ_{uts} - ultimate tensile strength, Δl - elongation, and ΔA - reduction in area), impact toughness (CVN - energy absorbed at fracture, Shear - percent plastic shear, and Lat. Exp. - lateral expansion of the Charpy specimen), and microstructure (PF - primary ferrite, AF - acicular ferrite, and FS - ferrite with second phases, aligned and non-aligned). The criteria of selection of the four specimens included all factors discussed so far: good electrode

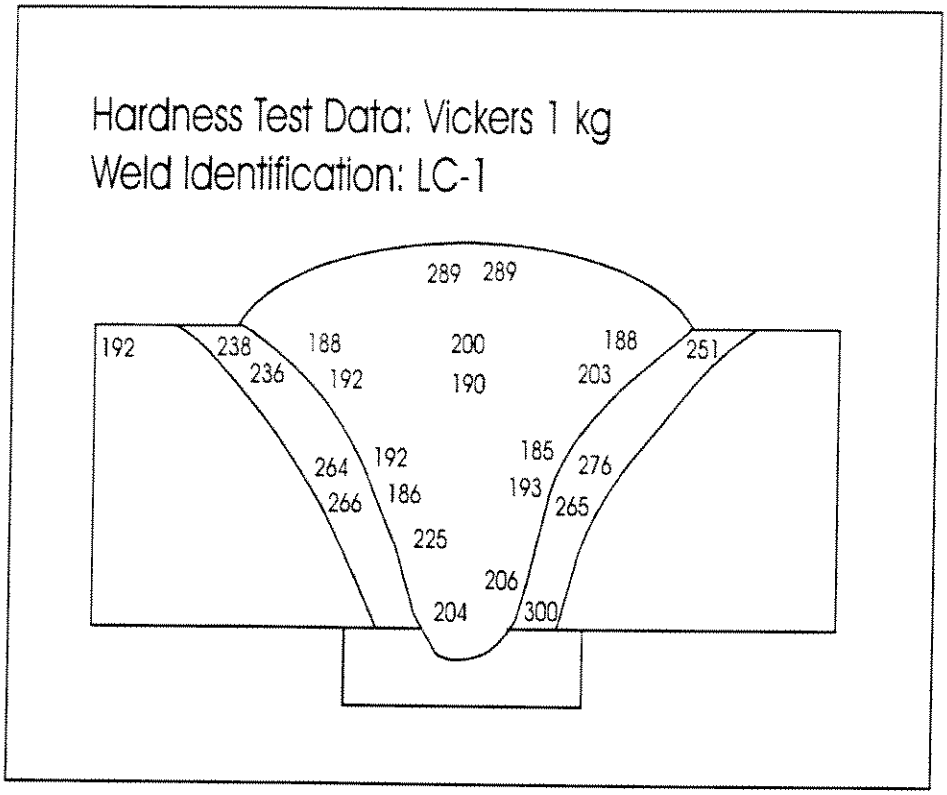

Figure 1. Schematic drawing of the transvers cross-section of a multiple pass wet weld indicating the locations and typical readings of the hardness measurements.

performance (eg., LC-2), good bend test results (eg., LC-11, UL-6), and expected significance of flux additions (eg., LC-11, UL-6, UL-12). The results of these tests are listed below in Table XII.

Table XII. Test results of four selected welds.

Weld	σ_y (ksi)	σ_{uts} (ksi)	Δl (pct.)	ΔA (pct.)	CVN② (ft-lb)	Shear (pct.)	Lat. Exp. (mils)	PF (vol.pct.)	AF (vol.pct.)	FS (vol.pct.)
LC-2	72.3	79.6	10	19	30	40	40	30	35	35
LC-2①	80.3	86.9	14.6	17.3	28/30	--	28	--	--	--
LC-11	81.2	86.2	2.9	5.7	26.6	30	30	13	63	24
UL-6	71.5	78.3	7.1	15.4	29.3	40.	33	17	35	48
UL-12	71.7	74.1	5.0	9.0	28.7	30	35	24	31	45

① Test performed by Global Divers, Inc.
② Test conducted at 28°F.

The low carbon steel electrode welds, in particular, LC-2, presented good tensile properties. An average elongation of 12.3 pct. (10/14.6 pct.) was obtained. Reduction in area of these specimens was equally good, approximately 18% (19/17.3%). Its impact energy was also excellent. Even though the tests were conducted at 28°F (below the 32°F required), the energy absorbed at fracture exceeded the requirment of 15 ft-lb established by the AWS D3.6 Specification. The other low carbon steel electrode weld, LC-11 performed well in strength properties (comparable to the LC-2 weld), but poorly in elongation, a mere 2.9 pct. This result is related to the oxygen content in the weld metal, 1550 ppm. The large number of inclusions is responsible for the low ductility. The impact energy of 27 ft-lb at 28°F was quite satisfactory.

The ultra-low carbon steel electrode welds performed reasonably well. The lower strength properties of the two welds were expected because of the lower carbon content in the core rod, 0.019 wt. pct. (maximum), as compared with 0.06 wt. pct. in the low carbon steel rods. Both welds presented low elongation, UL-6 with 7 pct. and UL-12 with 5 pct.. The high Fe-Mn addition weld, UL-12, in particular, exhibited only 9 pct. reduction in area. This result is related to the higher carbon and manganese recovery in the weld metal. Despite the dismal tensile properties of these ultra-low carbon steel electrode welds, their impact energies (29 ft-lb at 28°F) were, nevertheless, very good.

Figures 2 to 5 show the macro- and micrographs of the four welds. All welds showed a mixed microstructure of primary ferrite (grain boundary and blocky ferrite), acicular ferrite and FS (ferrite with aligned or non-aligned second phases). The FS phase included microstructural features such as martensite, bainite and MAC microconstituent. Both LC-2 and UL-6 displayed approximately 35 vol. pct. of acicular ferrite, which was responsible for their more ductile fracture appearance and higher Charpy impact toughness. It is generally agreed that acicular ferrite, with its short and randomly oriented laths, exhibits good strength and toughness. However, the presence of substantial amounts of FS phases in these welds imposed a limit to the toughness achievable. Lath martensite was also evident in the form of laths that maintain approximately 60° amongst themselves and appear as units of triangular configuration.

The apparent contradiction between the high acicular ferrite content (63 vol. pct.) and the low elongation (2.9 pct.) found in weld LC-11 can be attributed to two factors. First, the microstructural characterization work was performed on the top bead with the purpose of examining its microstructure as a function of the electrode composition. This procedure is extremely important for electrode development. Second, the mechanical properties of a multiple-pass weld depend on the properties of the reheated weld metal as well as those of the as-solidified weld metal. Often times, depending on the weld deposition schedule, the amount of reheated weld metal in a weld can be larger than the as-solidified weld metal. In this case, the top bead microstructure can not be related with the mechanical properties. Finally, the high carbon (0.134 wt. pct.) and manganese (0.81 wt. pct.) contents indicates the presence of lath martensite. The high silicon content (0.53 wt. pct.) also increases the embrittlement susceptibility of the weld metal which may result in low elongation.

None of the welds exhibited a large amount of acicular ferrite as reported by Sanchez-Osio, Ibarra, Liu, and Olson (over 60 vol. pct.). However, this result is not unexpected since the electrodes that these authors experimented had titanium and boron additions which improved significantly the performance of the welds.

3.8 Relationship between Electrode Properties and Flux Ingredients

To investigate the effects of Fe-Mn, $CaCO_3$ and ZrO_2 additions, the behavior of the fluxes and the weld properties were compared. Figures 6 to 8 show the weld metal oxygen content as a function of carbon, manganese and silicon. The "equilibrium" behavior of an inverse

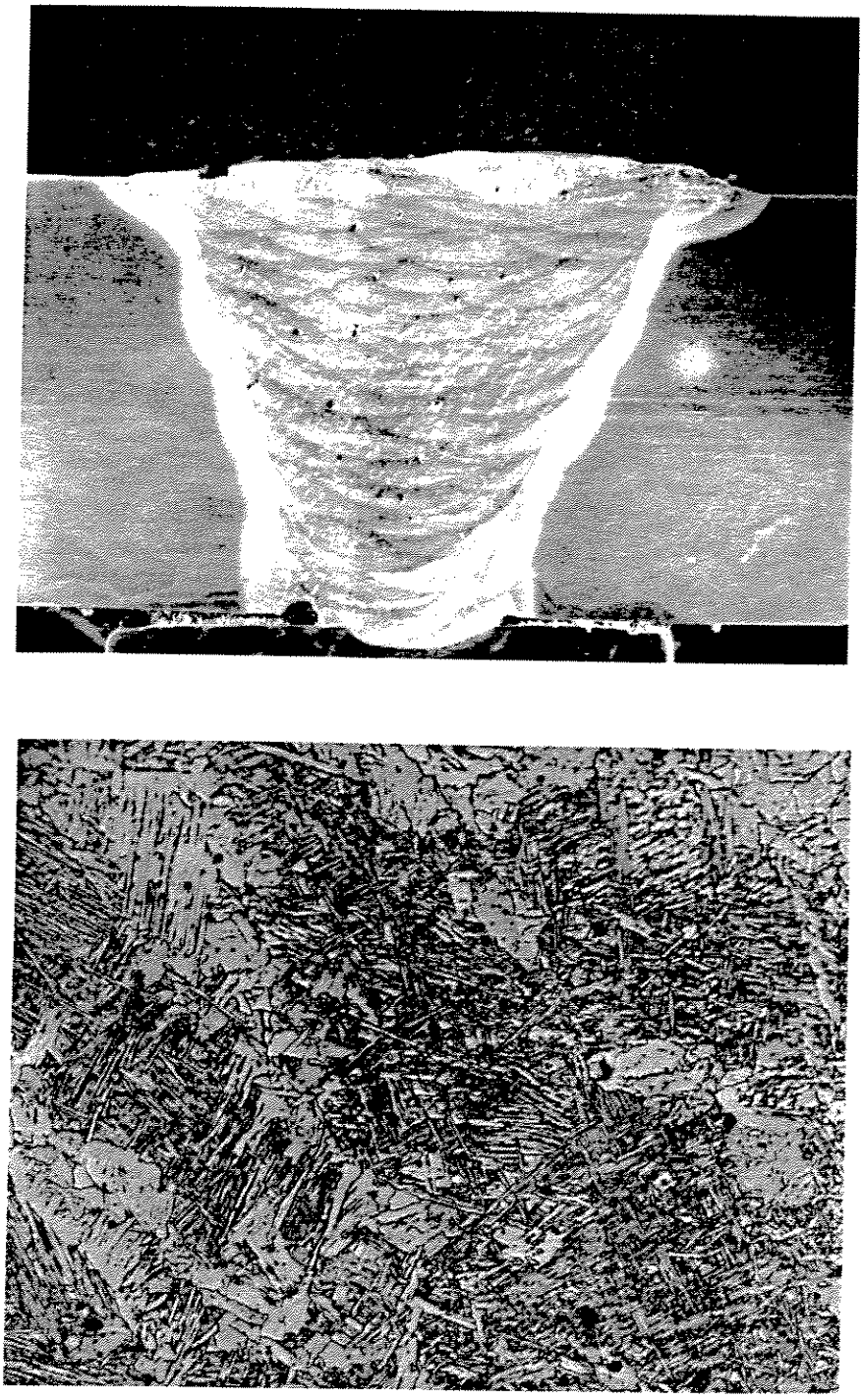

Figure 2. Macro- and micrograph of Weld LC-2 showing the bead deposition and microstructure of the top center bead. (Magnification: 3.75X and 500X, respectively.)

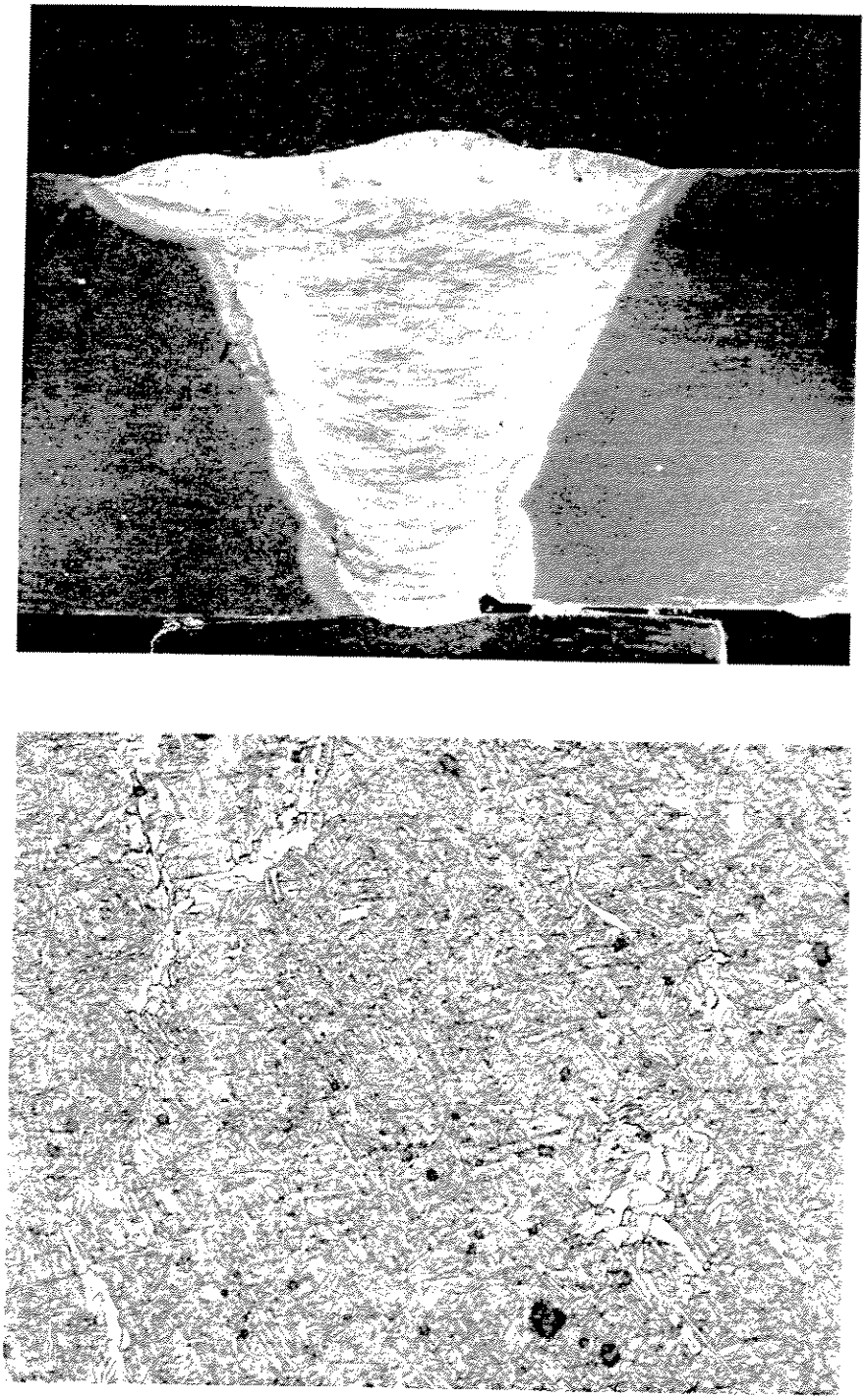

Figure 3. Macro- and micrograph of Weld LC-11 showing the bead deposition and microstructure of the top center bead. (Magnification: 3.75X and 500X, respectively.)

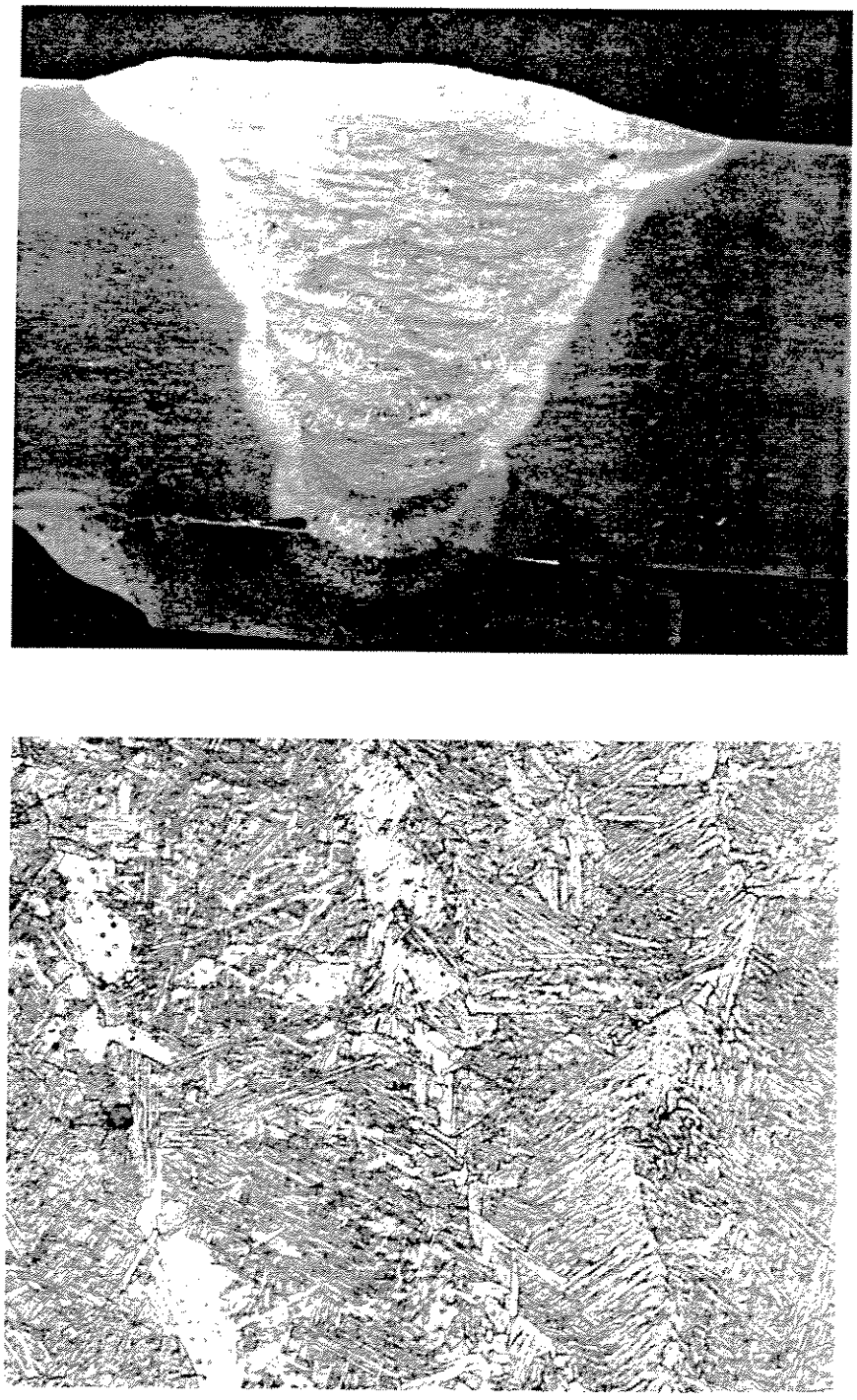

Figure 4. Macro- and micrograph of Weld UL-6 showing the bead deposition and microstructure of the top center bead. (Magnification: 3.75X and 500X, respectively.)

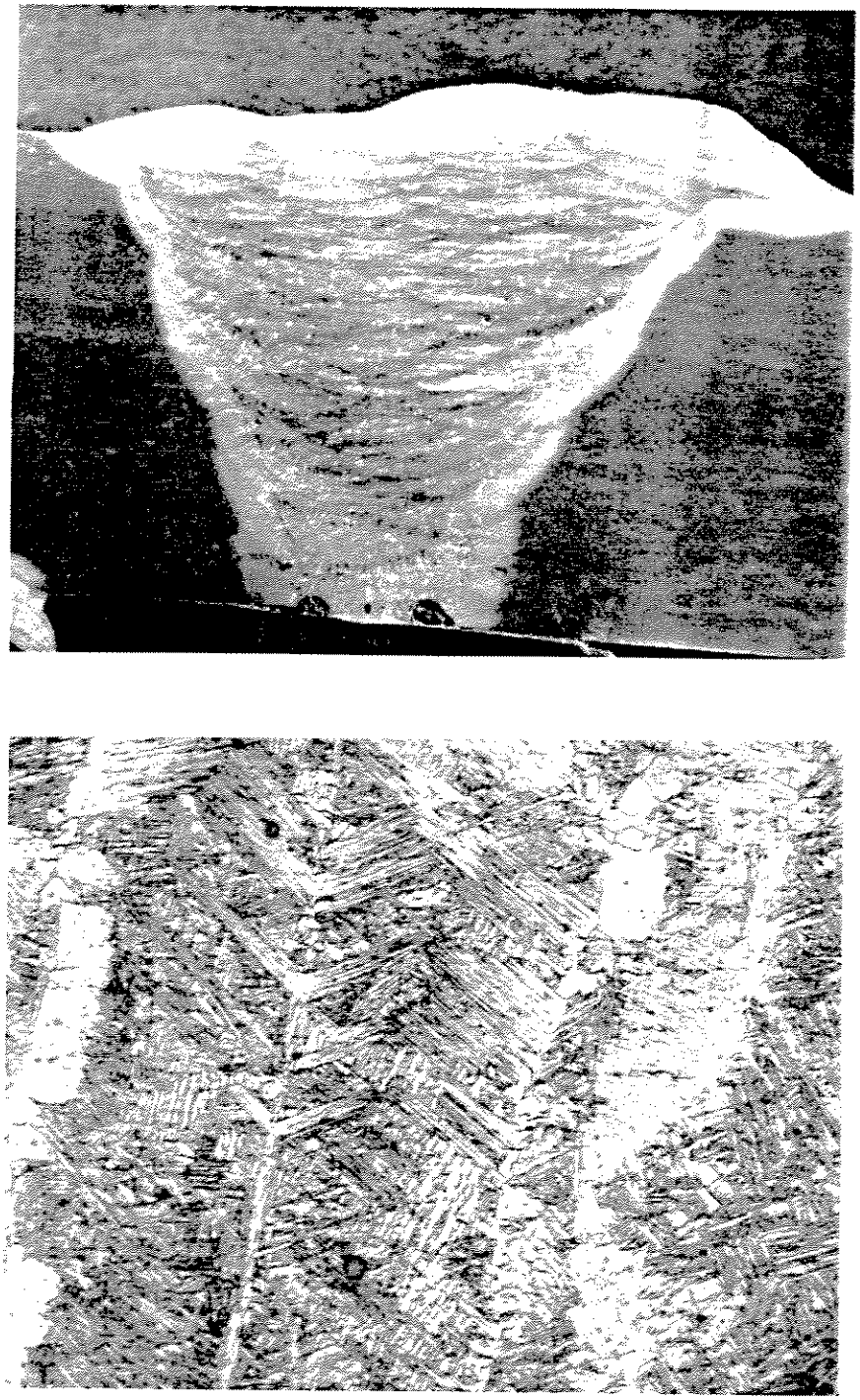

Figure 5. Macro- and micrograph of Weld LC-12 showing the bead deposition and microstructure of the top center bead. (Magnification: 3.75X and 500X, respectively.)

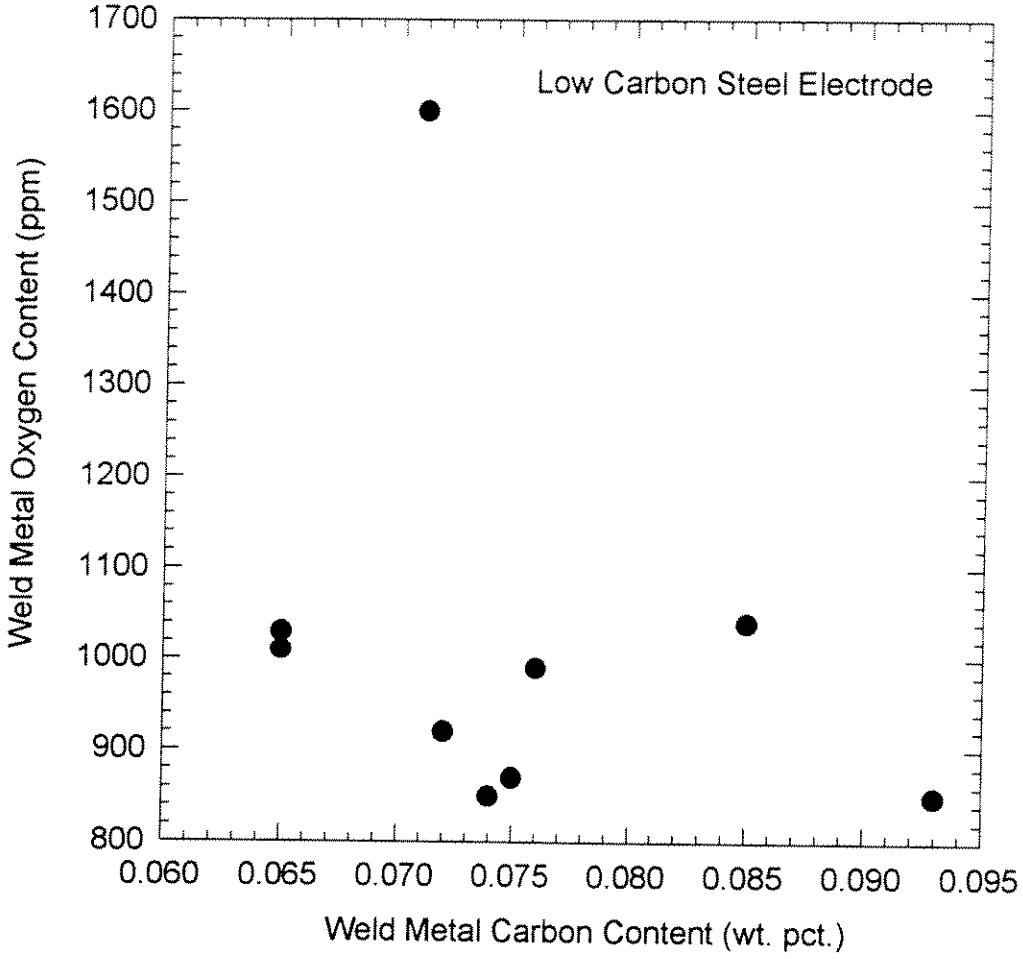

Figure 6. Oxygen content as a function of carbon content in the experimental wet welds.

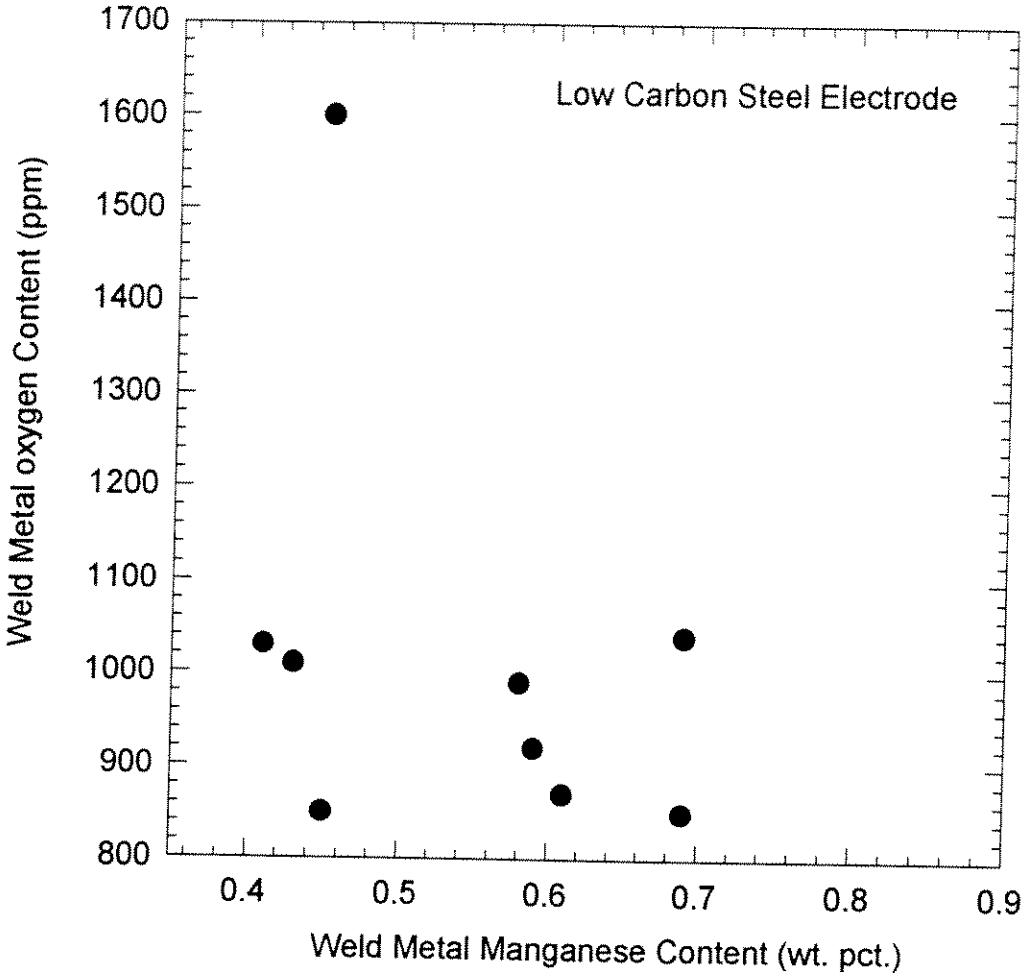

Figure 7. Oxygen content as a function of manganese content in the experimental wet welds.

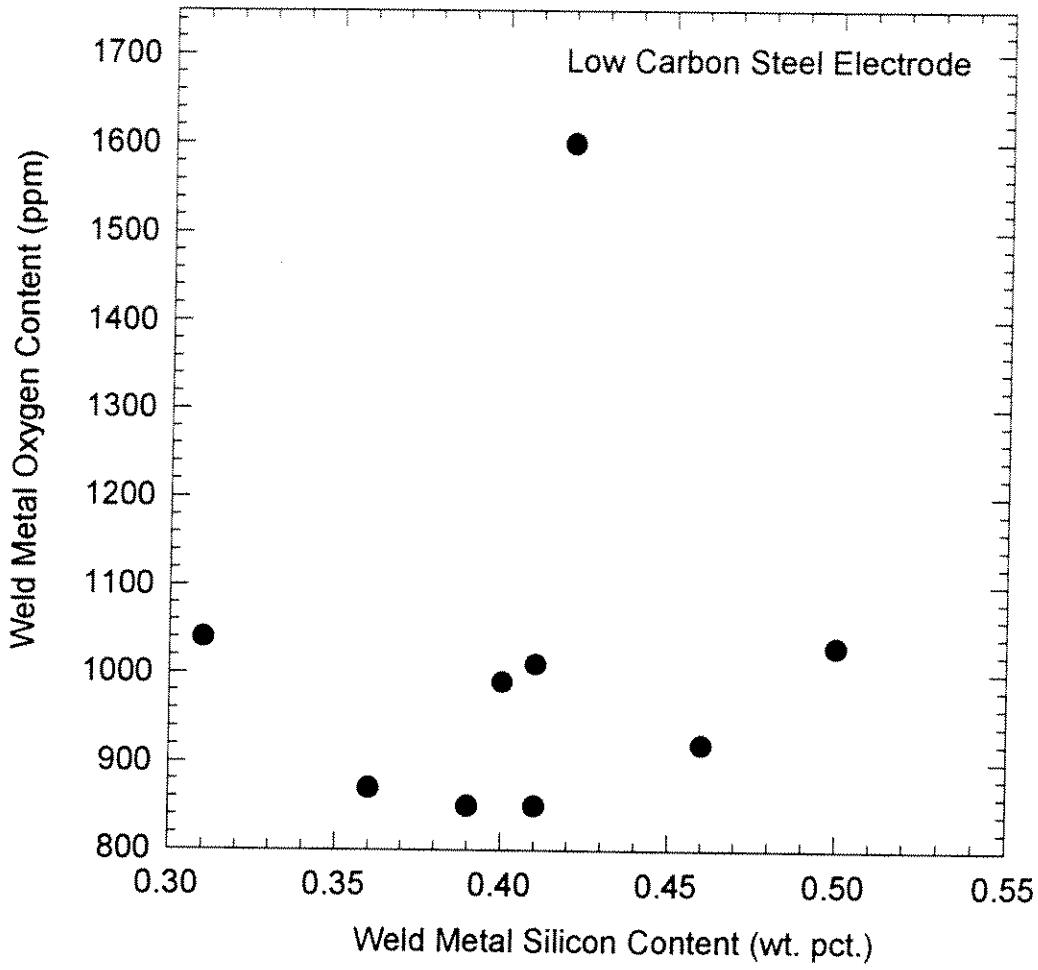

Figure 8. Oxygen content as a function of silicon content in the experimental wet welds.

relationship (for example, increasing oxygen content with decreasing manganese content) was not observed, which could be a result of the fast cooling rate of the wet welding process. However, a more likely cause of this non-conformity is that chemical analysis of the weld system included the determination of the alloying elements in both "combined" and "dissolved" state. Combining the two quantities of an alloying element will not yield the typical equilibrium relationship with oxygen represented by the hyperbolic function. Figure 9 supports the veracity of the above explanation. In this diagram, the abcissa depicts the hardenability effect of the alloy which is represented by the carbon equivalent equation (C + Mn/6). The coordinate of the figure shows the concentration of the inclusion formers (O + Si/4). Each silicon atom in a silicate ion is linked to four oxygen atoms, thus, requiring the factor of 1/4. This figure shows, with some scatter, the inverse relationship that was not observed in the other figures, demonstrating the control of weld metal oxygen by means of deoxidizers.

Another reason for the inconclusive correlations shown in Figures 6 to 8 is the simultaneous variation of $CaCO_3$, ZrO_2 and Fe-Mn in the flux systems. For better interpretation of the experimental results, pairs of welds with controlled additions as shown in Table XIII were selected. The flux systems were grouped into four categories: 1) low $CaCO_3$-low ZrO_2, 2) low $CaCO_3$-high ZrO_2, 3) high $CaCO_3$-low ZrO_2, and 4) high $CaCO_3$-high ZrO_2. Comparing group 1 with group 2, and group 3 with group 4 provided information about the effect of ZrO_2. The comparison between groups 1 and 3, and groups 2 and 4 contributed to the understanding of the effect of $CaCO_3$.

Table XIII. Effect of flux ingredients on weld metal chemical composition, weld quality, and electrode weldability.

Fluxes	Fe-Mn ①	$CaCO_3$ ①	ZrO_2 ①	C ②	O ③	Mn ②	Si ②	Porosity	Electrode Weldability ④
LC-1	8	3.2	5	0.071	1600	0.45	0.42	Class B	--
LC-7	12			0.072	920	0.59	0.46	Class A	
LC-8	8	3.2	8	0.065	1030	0.41	0.50	Class B	--
LC-2	12			0.085	1040	0.69	0.31	Class A	
LC-3	8	6.2	5	0.065	1010	0.43	0.41	Class B	--
LC-9	12			0.075	870	0.61	0.36	Class A	
LC-5/10	8	6.2	8	0.075	920	0.52	0.41	Class B	--
LC-12	14			0.093	850	0.69	0.39	Class A	

① Concentration in flux expressed in wt. Pct. ② Concentration in weld metal expressed in wt. pct.
③ Concentration in weld metal expressed in ppm. ④ See Tables VI and VII for comparison.

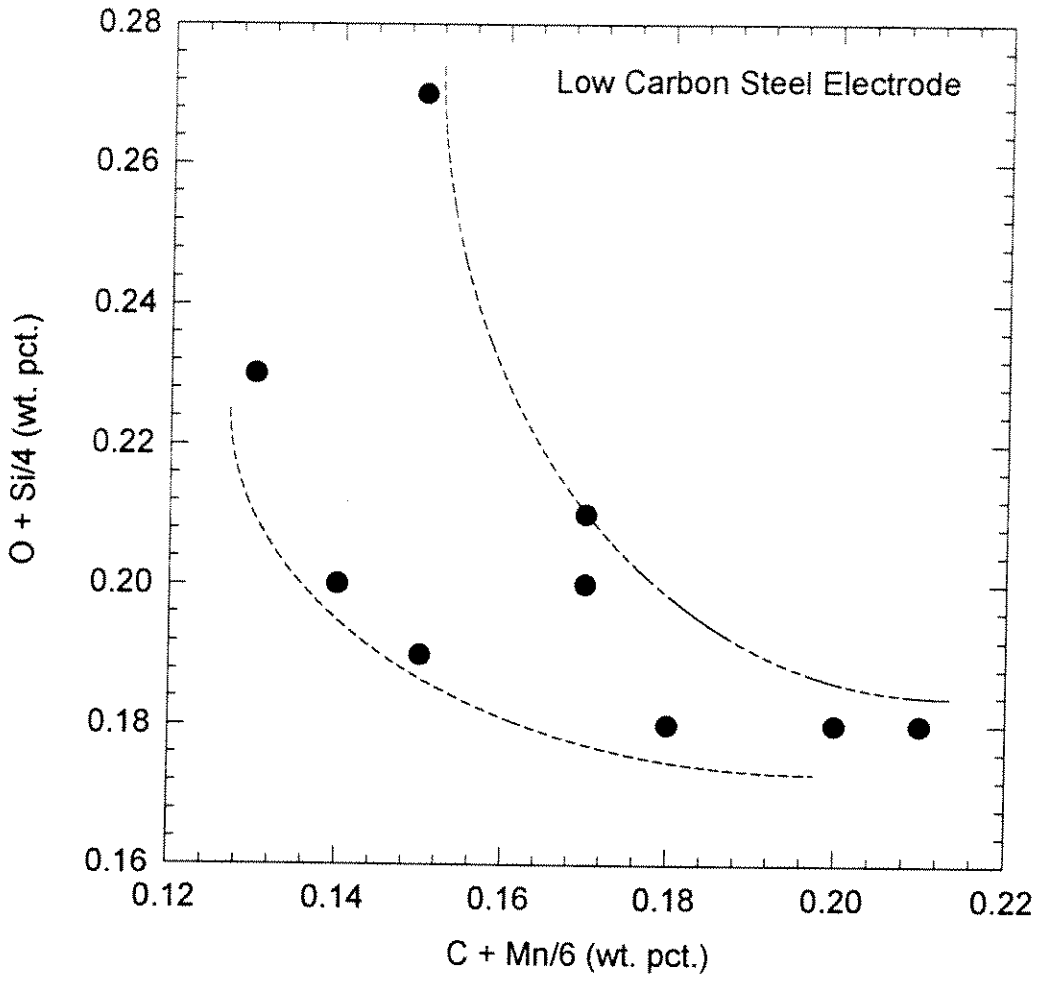

Figure 9. Inclusion formers as a function of hardenability agents in the experimental wet welds.

The effects of the flux additions on weld metal chemical composition can be better illustrated in Figures 10 to 13. As explained in previous sections, these graphs are organized by groups of low and high $CaCO_3$, and low and high ZrO_2. In the case of low $CaCO_3$ and low ZrO_2, the two flux systems chosen for discussion are LC-1 and LC-7. For low $CaCO_3$ and high ZrO_2, the fluxes are LC-8 and LC-2. Fluxes LC-3 and LC-9 were selected to represent the group with high $CaCO_3$ and low ZrO_2. Finally, for high $CaCO_3$ and ZrO_2 fluxes, LC-5/LC-10 and LC-12 were the ones used in the following discussion.

Figure 10 clearly shows the effect of Fe-Mn on weld metal manganese content. Increasing Fe-Mn in the flux increased the weld metal manganese content. Manganese recovery in the weld metal was between 6.8 to 8.7%. It is also important to note that when the oxygen potential of the flux system is increased, either by $CaCO_3$ and/or ZrO_2 increase, the increase in manganese with Fe-Mn increase became less. Especially in the case of 14 wt. pct. of Fe-Mn in the high $CaCO_3$ and high ZrO_2 flux system, the recovery of manganese was much lower.

Figure 11 shows the effect of Fe-Mn on weld metal carbon content. Results similar to weld metal manganese were observed. That is, weld metal carbon content increased with Fe-Mn addition, and that the increase became smaller in the presence of higher oxygen potential fluxes. Figure 12 plots weld metal silicon content with Fe-Mn addition in the flux. Notice the different behavior observed that silicon decreased with Fe-Mn addition. However, the behavior of silicon is difficult to interpret since silicon may exist in the form of solid-solution or combined silicate. This explanation has been presented earlier in Figure 9. To distinguish between "acid-soluble" (in solution) and "acid-insoluble" (in inclusions) contents of silicon would require an elaborated analytical program.

The net balance of manganese, carbon and silicon (gain or loss) with Fe-Mn addition can be seen in Figure 13 when weld metal oxygen is plotted as a function of Fe-Mn addition. In the case of low $CaCO_3$ (3.2 wt. pct.) and low ZrO_2 (5 wt. pct.) in the flux, oxygen decreased significantly with Fe-Mn addition. Increasing $CaCO_3$ and ZrO_2 in the flux to 6.2 and 8 wt. pct., respectively, the addition of Fe-Mn did not result in any significant reduction in weld metal oxygen. This observation clearly indicates that the oxygen potential of a flux plays an important role in the final oxygen content of the weld pool. Higher oxygen potential will reduce the efficiency of ferro-alloy additions, thus the smaller reductions observed.

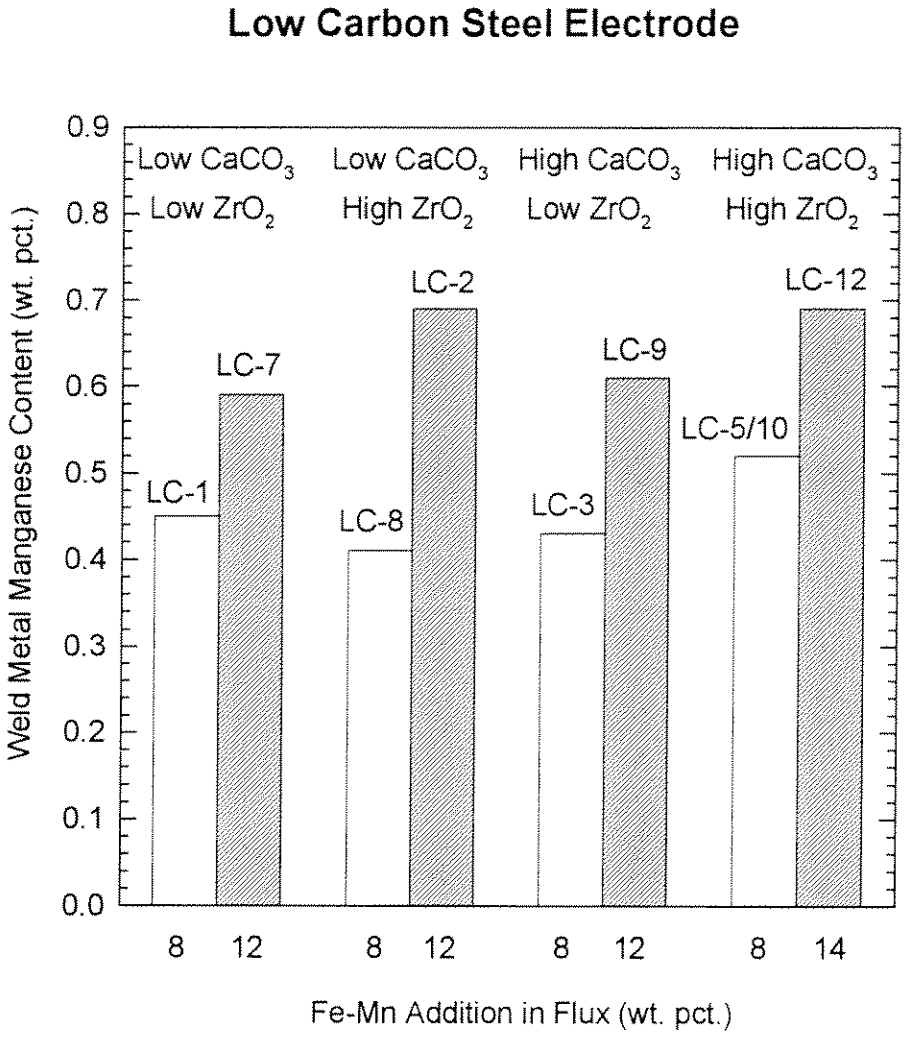

Figure 10. Effect of Fe-Mn, $CaCO_3$ and ZrO_2 additions on weld metal manganese content.

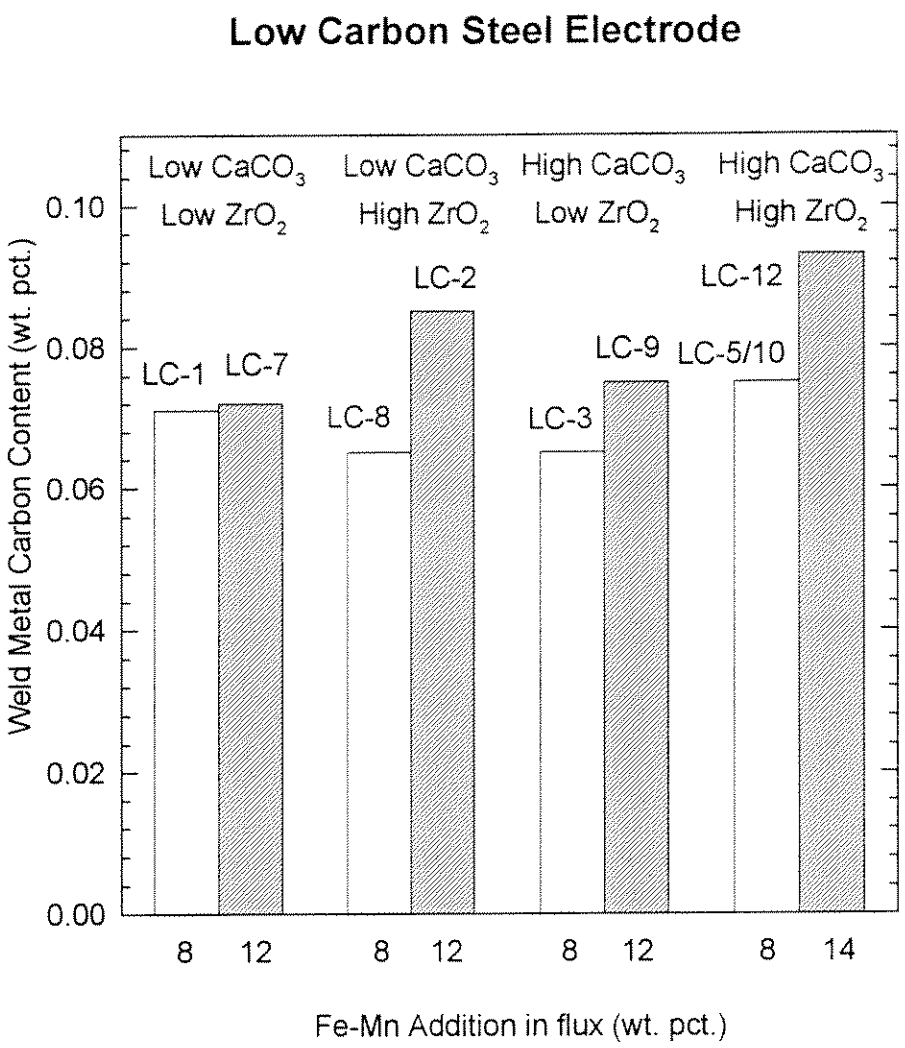

Figure 11. Effect of Fe-Mn, $CaCO_3$ and ZrO_2 additions on weld metal carbon content.

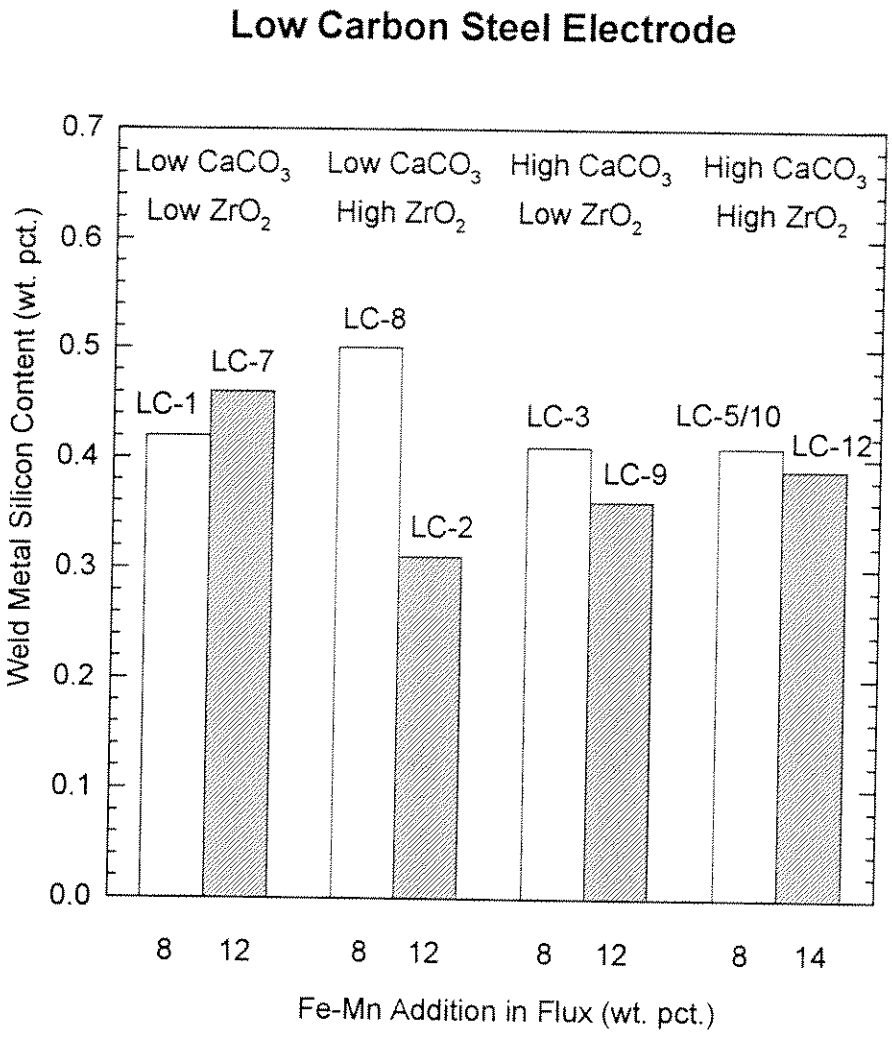

Figure 12. Effect of Fe-Mn, $CaCO_3$ and ZrO_2 additions on weld metal silicon content.

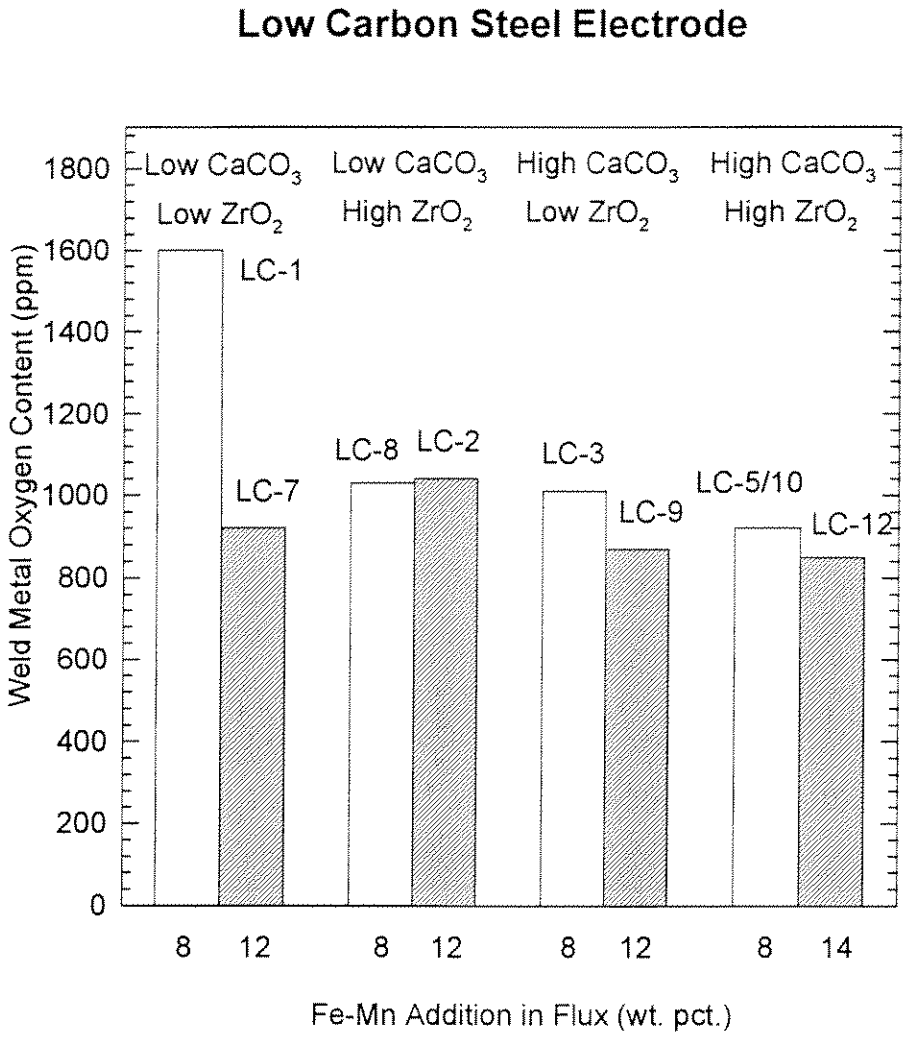

Figure 13. Effect of Fe-Mn, $CaCO_3$ and ZrO_2 additions on weld metal oxygen content.

In terms of bend test results, Figure 14 shows that Fe-Mn addition is mostly beneficial. For the welds made with LC-3, LC-9, LC-8, and LC-2 electrodes, an increase in Fe-Mn, from 8 to 12 wt. pct., decreased the bend radius, meaning that the samples were successfully bent to a greater curvature. Improper balance of flux oxygen potential and ferro-alloy additions in the high $CaCO_3$ and high ZrO_2 system (LC-5, LC-10 and LC-12) can lead to excessive increase in carbon and manganese which affects the microstructure, toughness and bend radius. Comparison between LC-1 and LC-7, with weld metal oxygen decreasing from 1600 to 800 ppm and increasing bend curvature at failure, also indicates an improper balance between manganese and oxygen in these welds.

The effect of oxygen on Charpy-V-notch impact toughness can also be seen in Figure 15. With increasing weld metal oxygen, the amount of energy abosorbed at fracture was observed to decrease.

Figure 16 shows that Fe-Mn additions increased the weld metal hardness of all the welds considered. The flux LC-12 provided with the most increase in hardness which agreed with the high magnanese and carbon recovery. The effect of hardenability elements is also illustrated in Figure 17 by the excellent correlation observed between average weld metal hardness and carbon equivalent. The effect of oxygen (inclusion formers) is not as clear, Figure 18. However, despite the wide scatter band, the data showed a decreasing trend of hardness with "oxygen". The scatter observed can be explained by the fact that silicon may be present in the form of solid-solution or inclusions. The silicon "in solution" tends to increase the hardness whereas the silicon "in inclusions" does not.

Similar analysis as described in the previous sections has also been performed for the UL specimens. In general, the findings agreed with those reported for the LC series welds. However, the large variations in weld metal composition and properties observed indicate that the weld pool perturbation as a result of lower carbon input and C-O "equilibrium" shift was much greater than that expected.

4. SELECTION OF TARGET FLUX SYSTEM

Based on the results presented in the previous sections, LC-2 was identified as the flux system that has the greatest potential for successful wet welding at the conditions tested. The flux

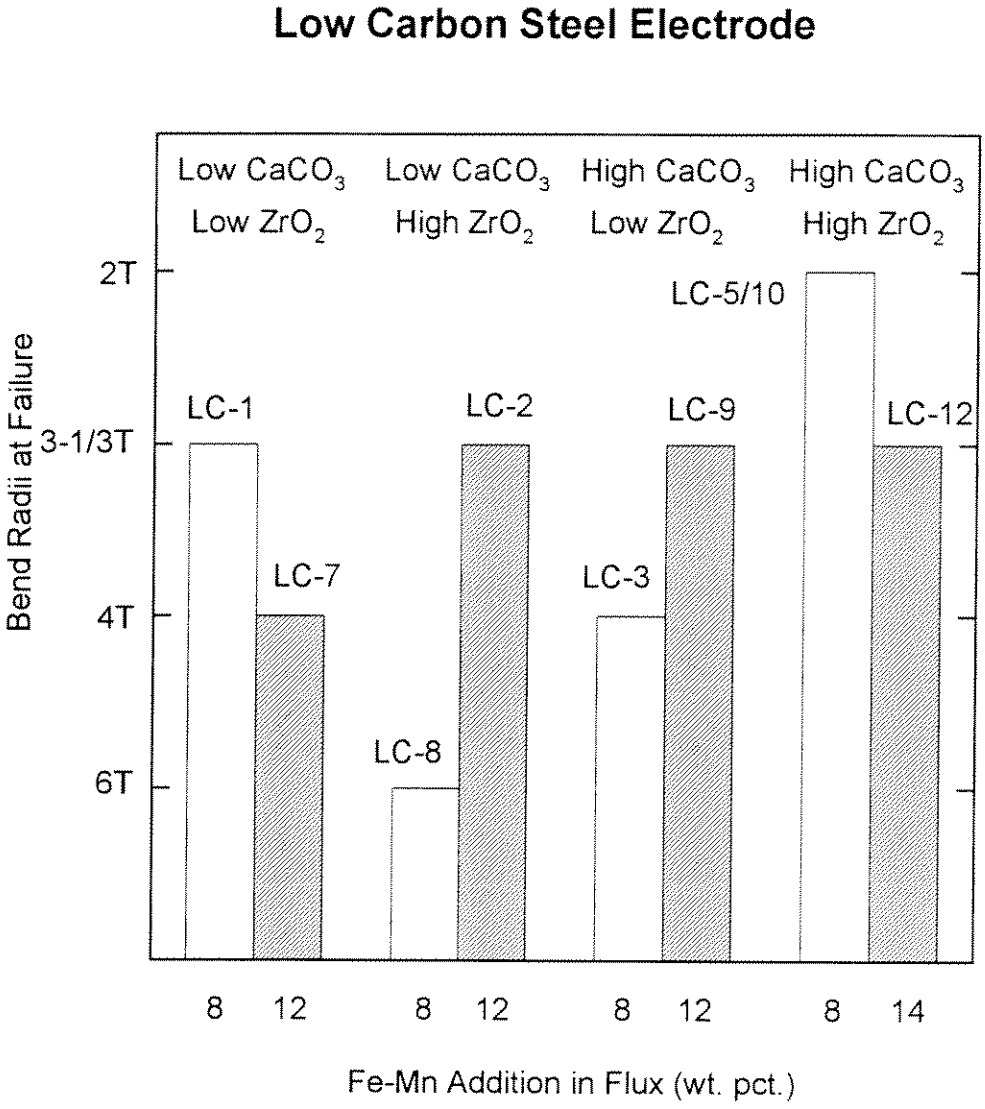

Figure 14. Effect of Fe-Mn, $CaCO_3$ and ZrO_2 additions on the bend radii at failure of the experimental wet welds.

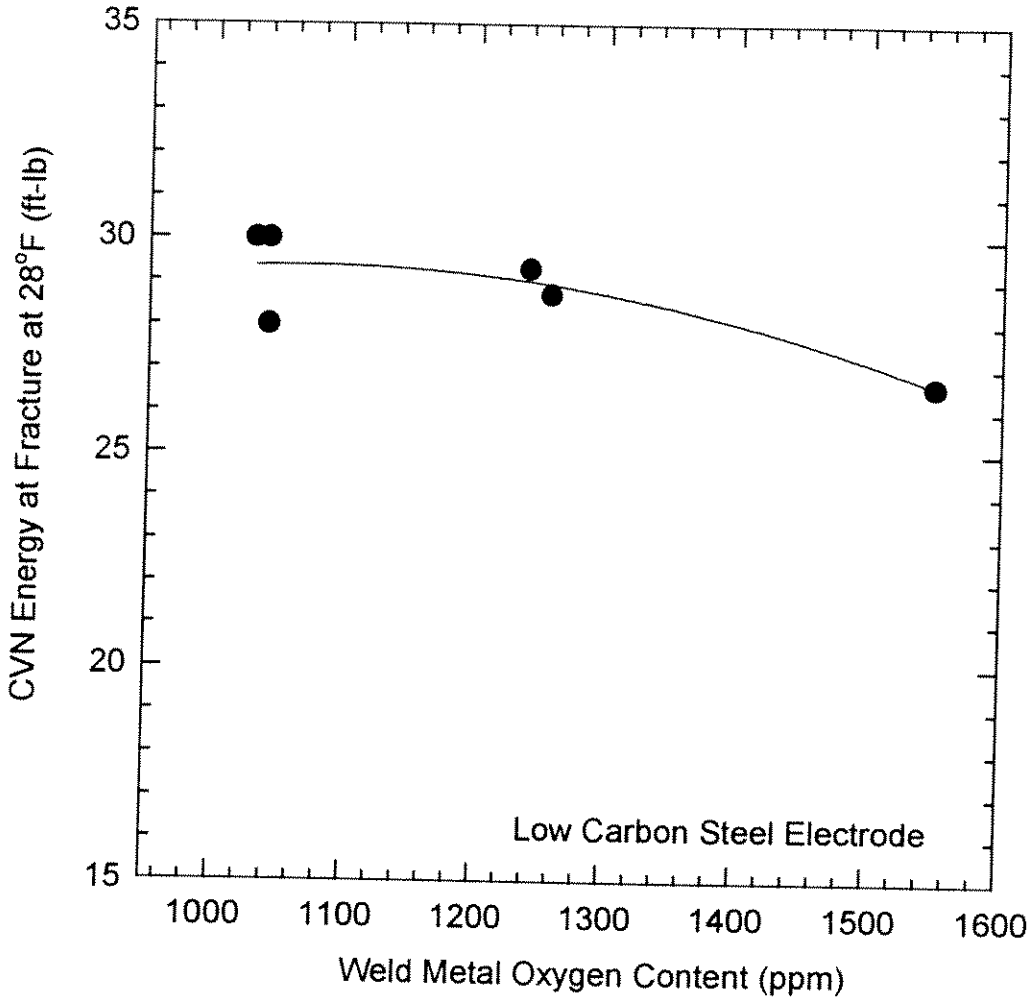

Figure 15. Effect of weld metal oxygen on CVN impact energy at fracture at 28°F of the experimental wet welds.

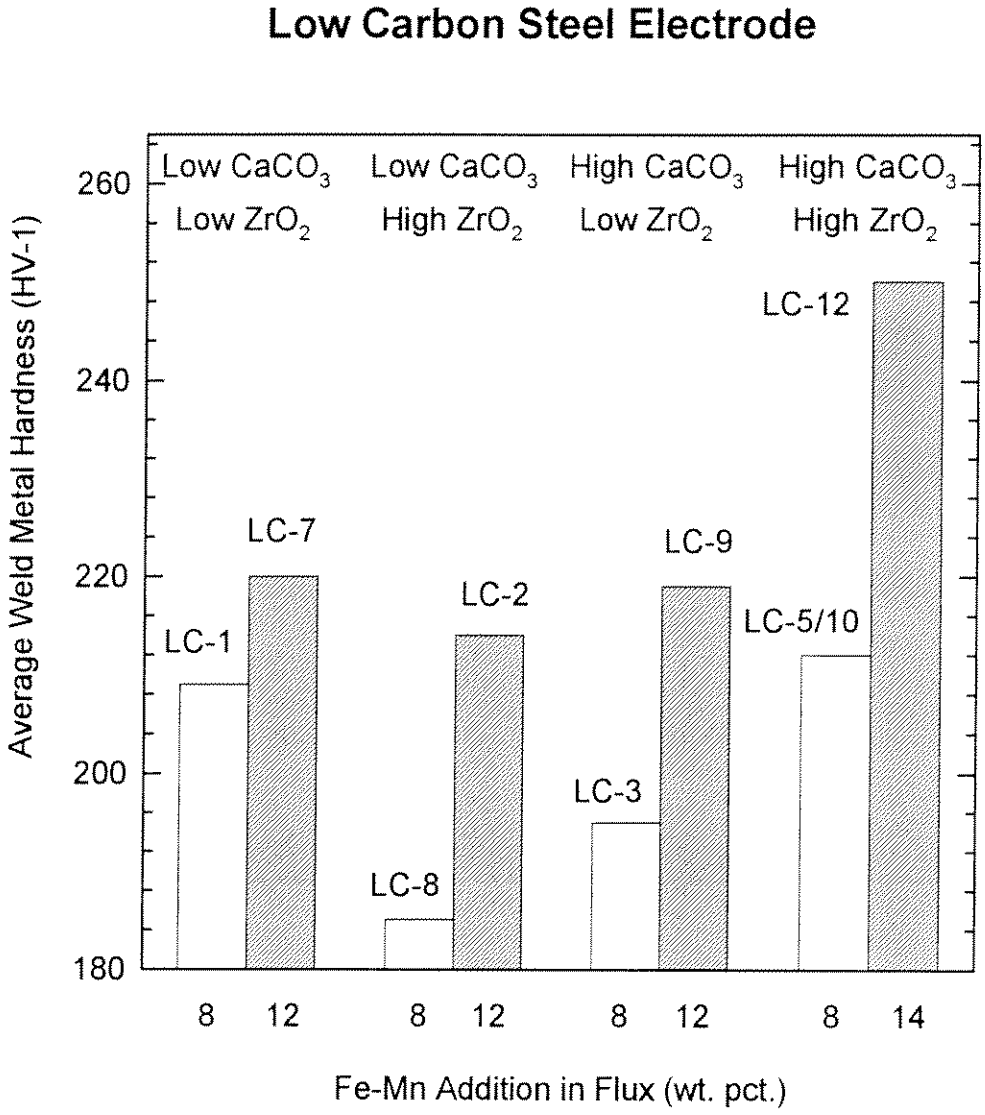

Figure 16. Effect of Fe-Mn, $CaCO_3$ and ZrO_2 additions on average weld metal hardness.

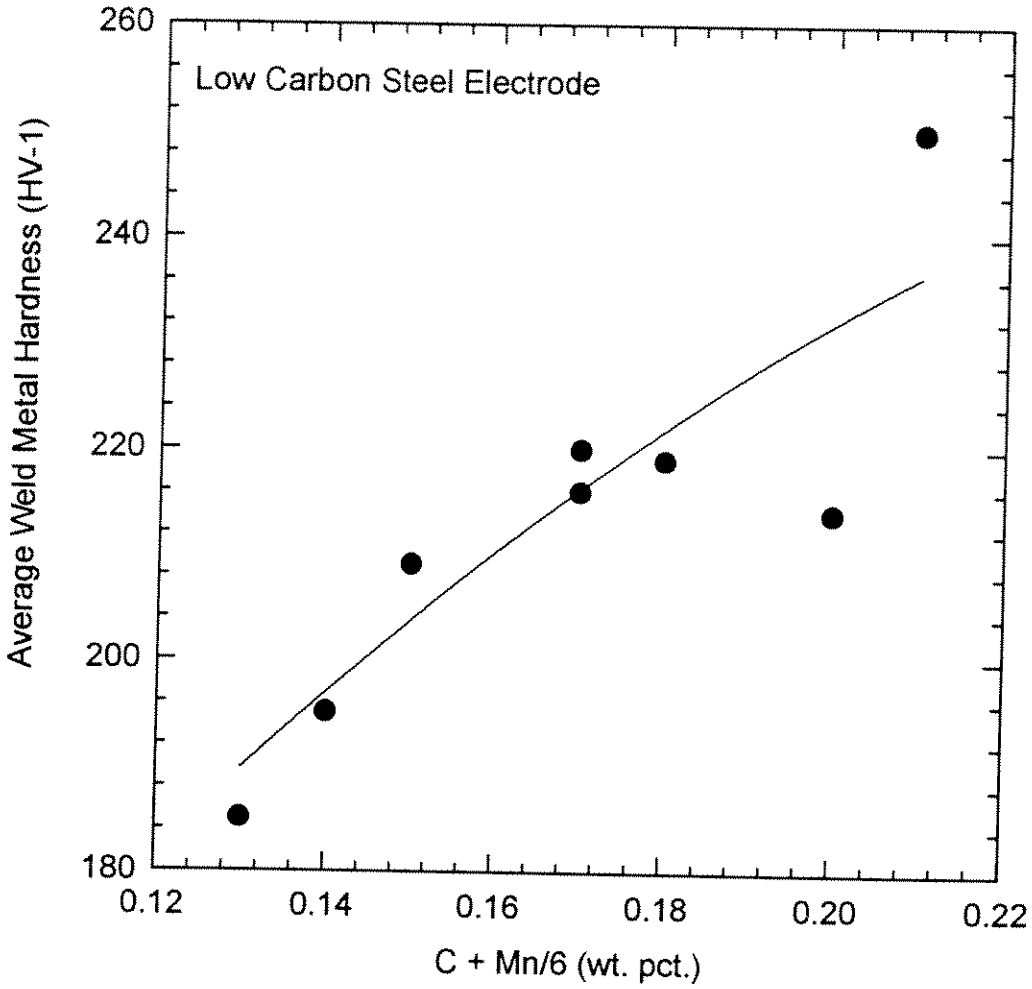

Figure 17. Effect of weld metal hardenability on average weld metal hardness.

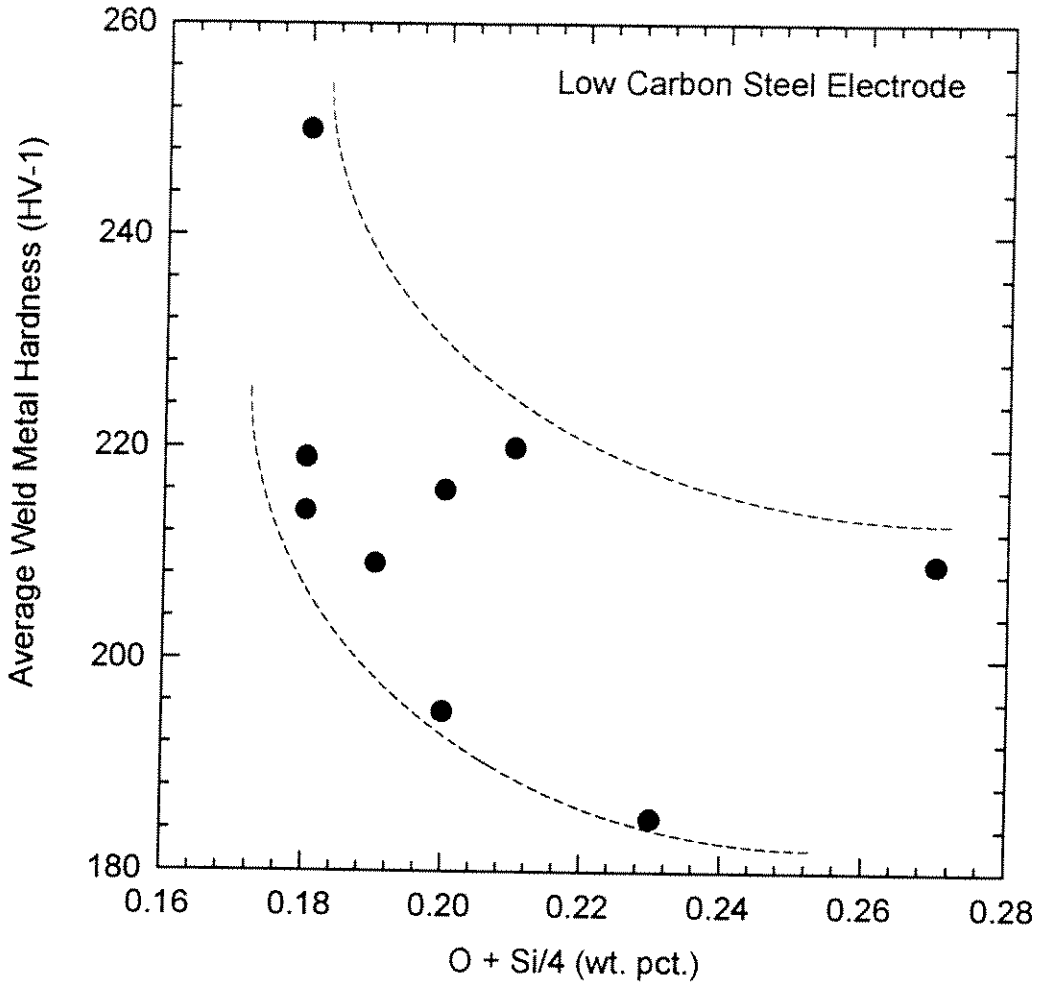

Figure 18. Effect of inclusion formers on average weld metal hardness.

had 3.2 wt. pct. $CaCO_3$, 8 wt. pct. ZrO_2, 12 wt. pct. Fe-Mn, in addition to the other ingredients as listed in Table I. The flux produced weld metal with high manganese content, 0.69 wt. pct., low silicon content, 0.31 wt. pct., low carbon content, 0.085 wt. pct., and average oxygen content, 1040 ppm, which resulted in a microstructure that exhibited high yield and tensile strength, high elongation, and high Charpy impact toughness. These properties can be attributed to the proper balance of weld metal oxygen and alloying content. The CSM-CWJR research team recommends LC-2 as the target flux for further testing.

5. RESEARCH PERSONNEL

This research work was performed by the following researchers:

a) Prof. Stephen Liu - CSM-CWJR
b) Prof. David L. Olson - CSM-CWJR
c) Mr. Charles Johnson, M.S. Candidate - CSM-CWJR

6. SUGGESTIONS FOR FURTHER INVESTIGATION

a) Several flux systems behaved extremely well in the present program and should be re-visited for fine tuning. An example of such a system is LC-5. The electrode exhibited great arc stability and the chemical composition of the weld metal was well balanced with 0.076 wt. pct. carbon, 0.58 wt. pct. manganese, 0.40 wt. pct. silicon, and 990 ppm oxygen. The bend test results were also good. The only reason for not selecting this electrode is the amount of porosity present in the weld. However, LC-5 would be a close second to be fine tuned for excellent wet welding performance.
b) Despite the excellent results obtained in the present program, a major drawback is the shallow depth, -33 ft. The same testing program must be carried out for greater depths, -100 ft., -200 ft., and -300 ft. to investigate the behavior of the proposed electrode(s).
c) To significantly elevate the quality and reliability of wet welding consumables for deep water applications, the use of titanium and boron must be explored. Initital studies have been carried by CSM researchers that the weld metal microstructure is much improved, with a three fold increase of acicular ferrite. The amount of lath martensite also decreased

correspondingly. Optimal additions fo titanium and boron in the target flux system, LC-2, will produce excellent quality wet weld quality for deep water welding.

d) While analyzing the current data, the authors experienced some difficulty in correlating bend test data with elongation data and Charpy-V-notch impact test data. The relationship between ductility and toughness must be established for better understanding of the significance of the results of these tests and how to describe the quality of wet welds.

7. ACKNOWLEDGMENT

The authors acknowledge the support of the Joint Industry Program in conducting this research program.

8. APPENDIX

8.1 Experimental weld hardness data.

Hardness Test Data: Vickers 1 kg
Weld Identification: LC-1

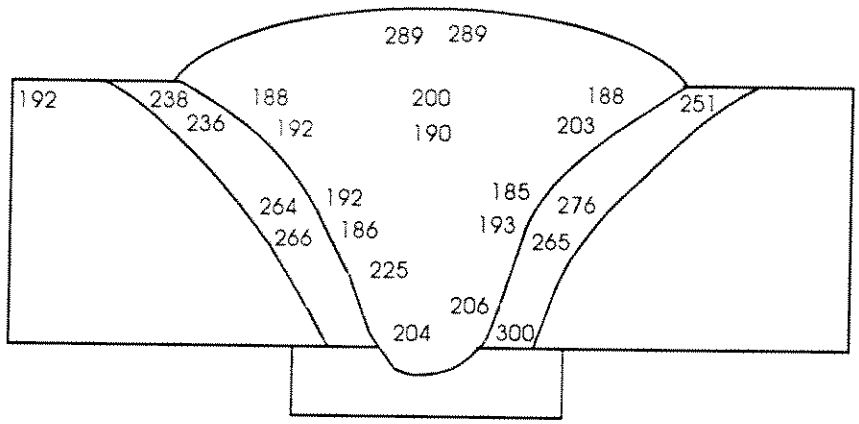

Hardness Test Data: Vickers 1 kg
Weld Identification: LC-2

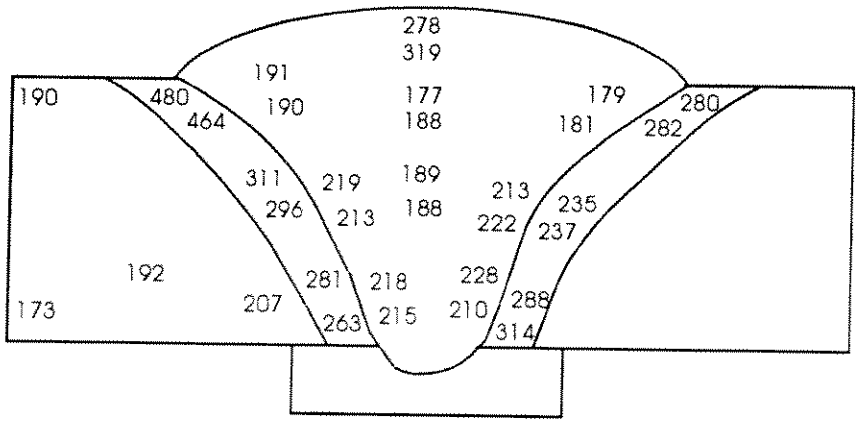

Hardness Test Data: Vickers 1 kg
Weld Identification: LC-3

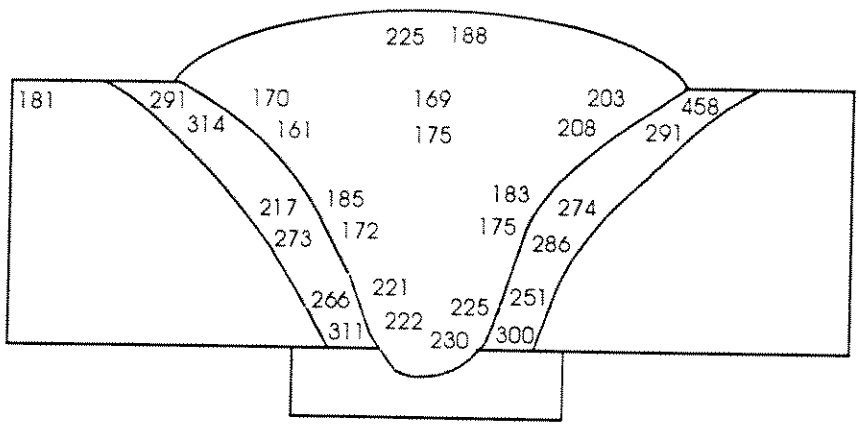

Hardness Test Data: Vickers 1 kg
Weld Identification: LC-4

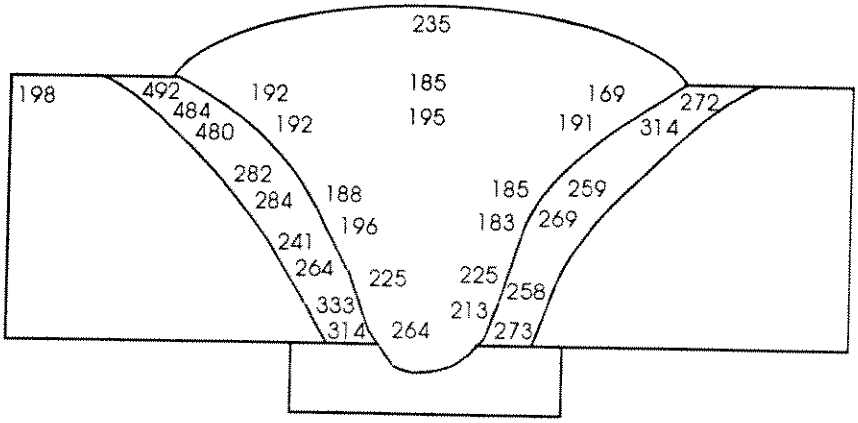

Hardness Test Data: Vickers 1 kg
Weld Identification: LC-5

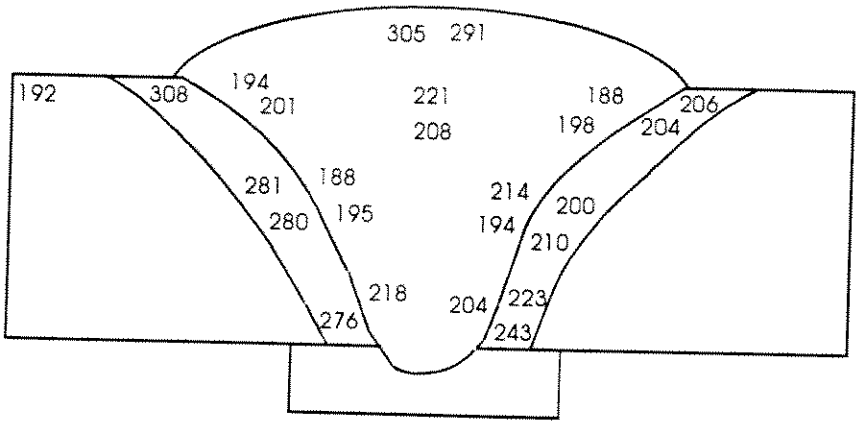

Hardness Test Data: Vickers 1 kg
Weld Identification: LC-6

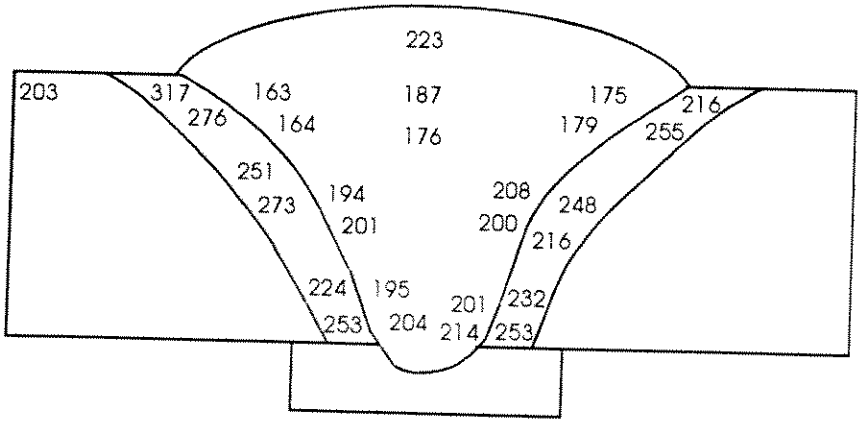

Hardness Test Data: Vickers 1 kg
Weld Identification: LC-7

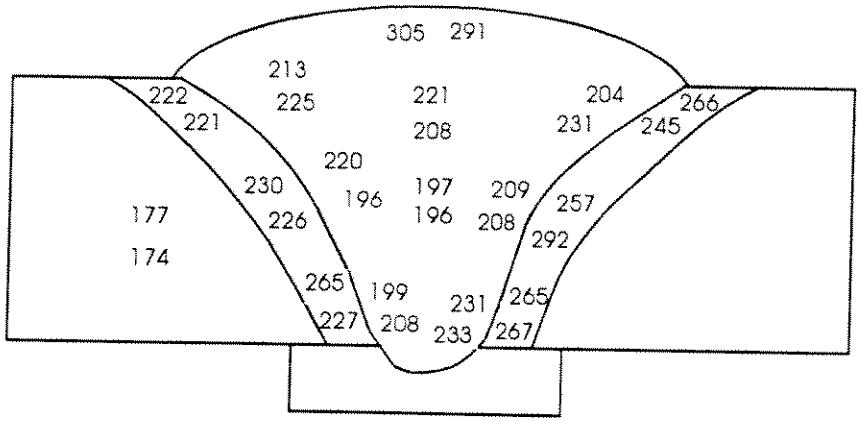

Hardness Test Data: Vickers 1 kg
Weld Identification: LC-8

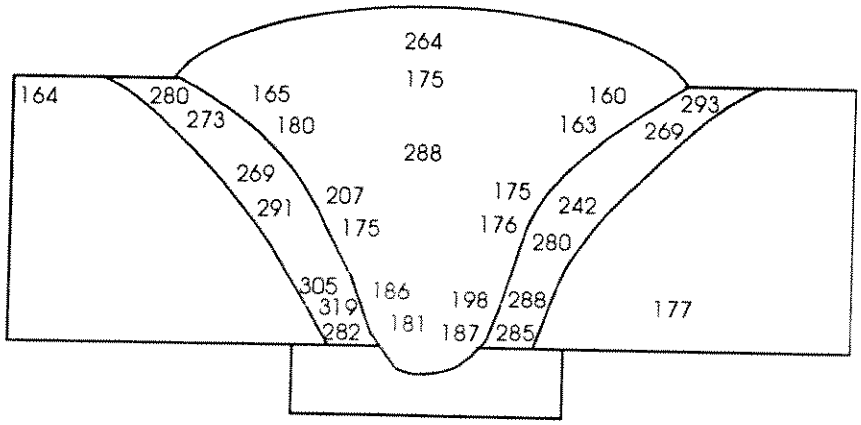

Hardness Test Data: Vickers 1 kg
Weld Identification: LC-9

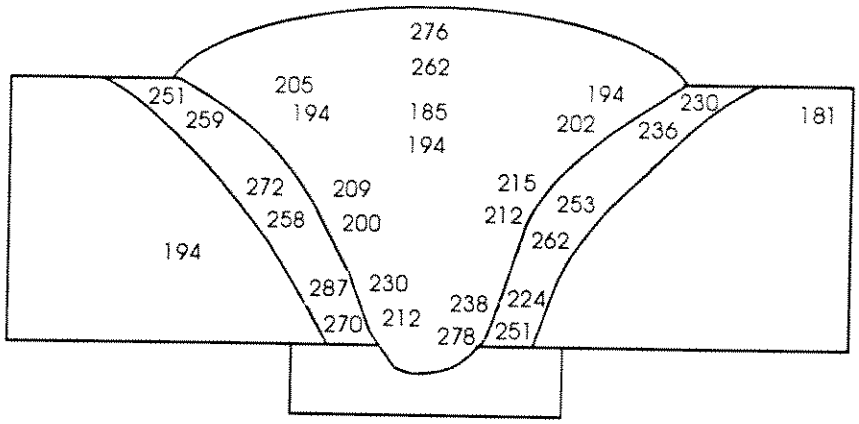

Hardness Test Data: Vickers 1 kg
Weld Identification: LC-10

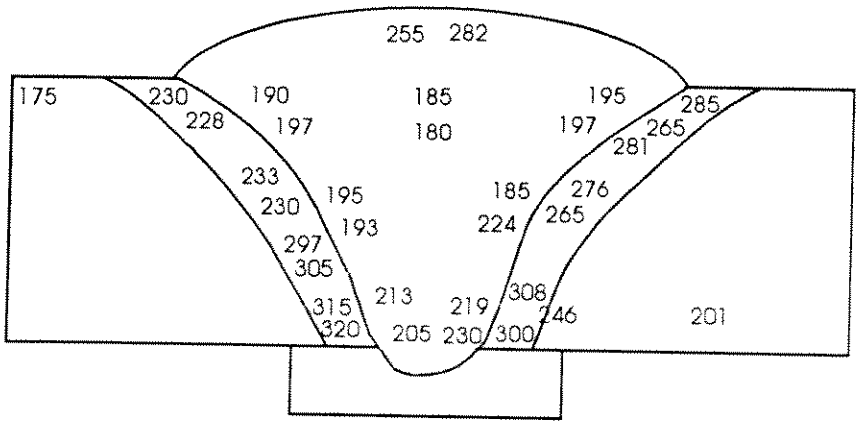

Hardness Test Data: Vickers 1 kg
Weld Identification: LC-11

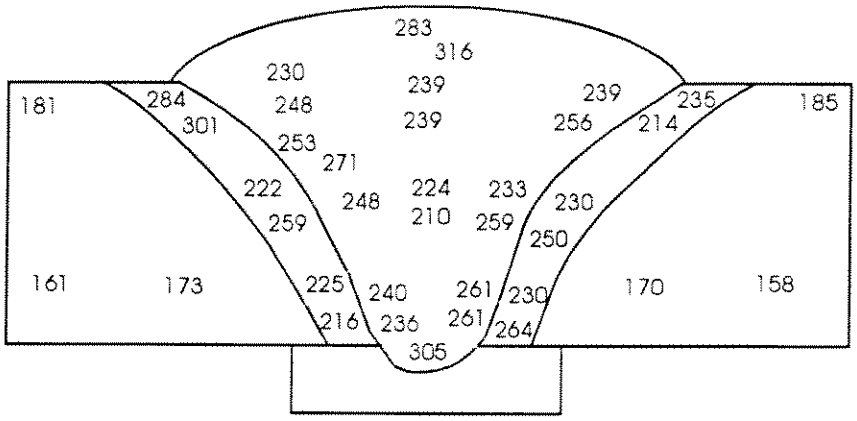

Hardness Test Data: Vickers 1 kg
Weld Identification: LC-12

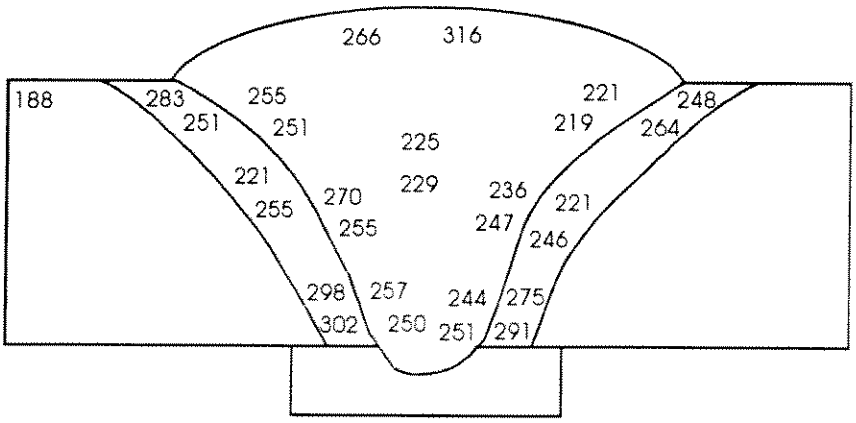

Hardness Test Data: Vickers 1 kg
Weld Identification: UL-1

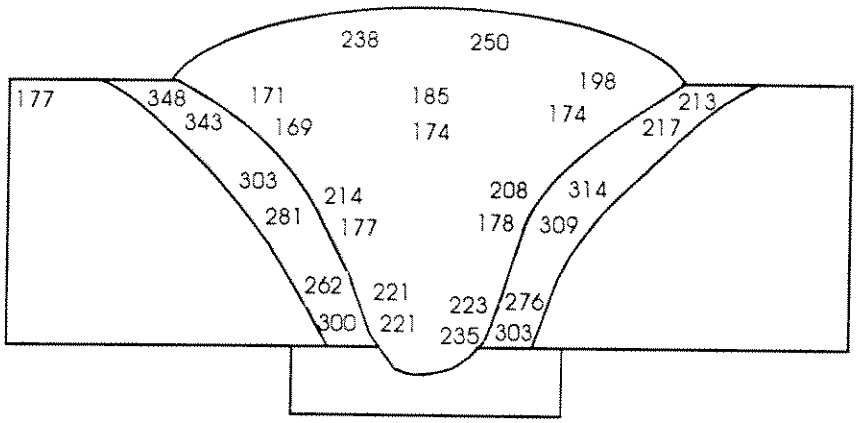

Hardness Test Data: Vickers 1 kg
Weld Identification: UL-2

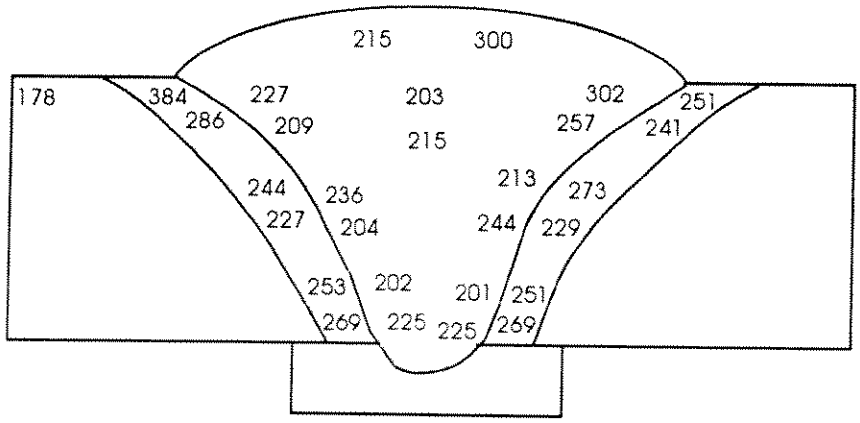

Hardness Test Data: Vickers 1 kg
Weld Identification: UL-3

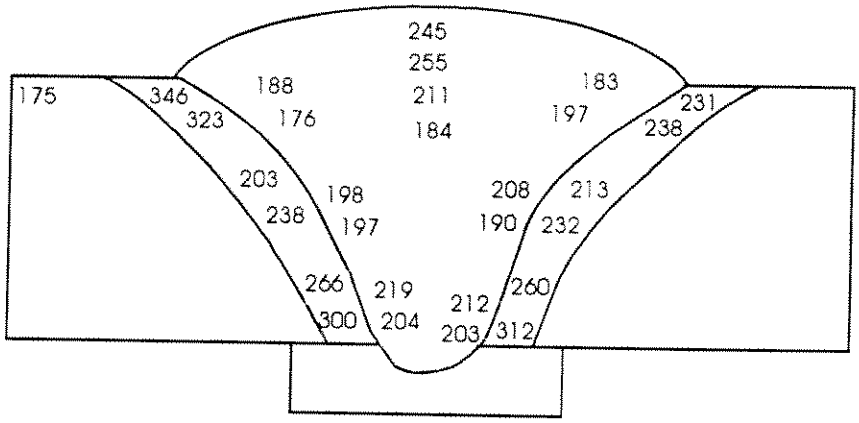

Hardness Test Data: Vickers 1 kg
Weld Identification: UL-4

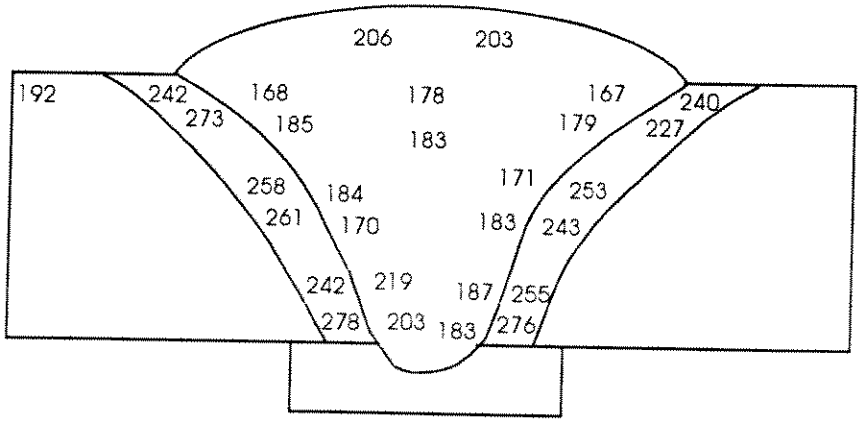

Hardness Test Data: Vickers 1 kg
Weld Identification: UL-5

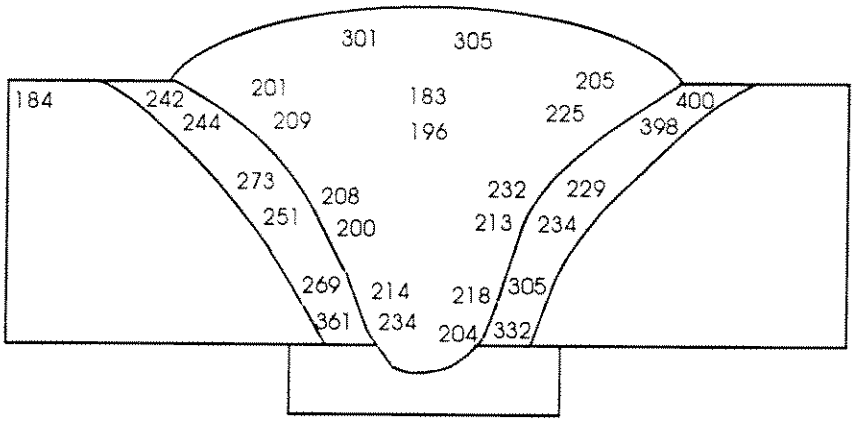

Hardness Test Data: Vickers 1 kg
Weld Identification: UL-6

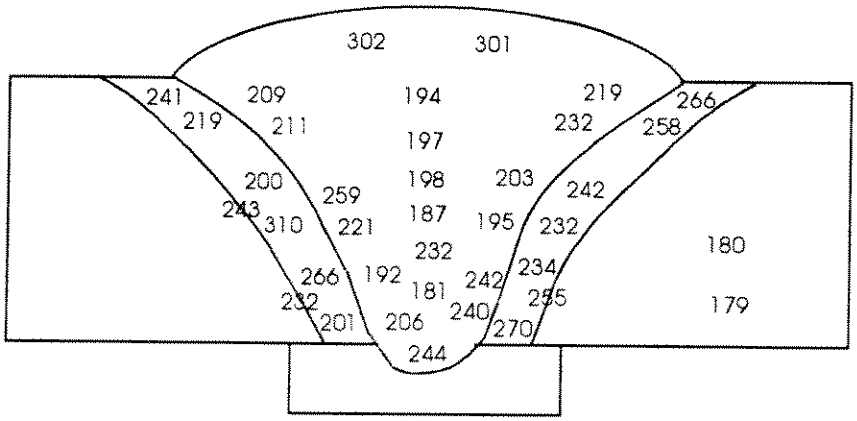

Hardness Test Data: Vickers 1 kg
Weld Identification: UL-7

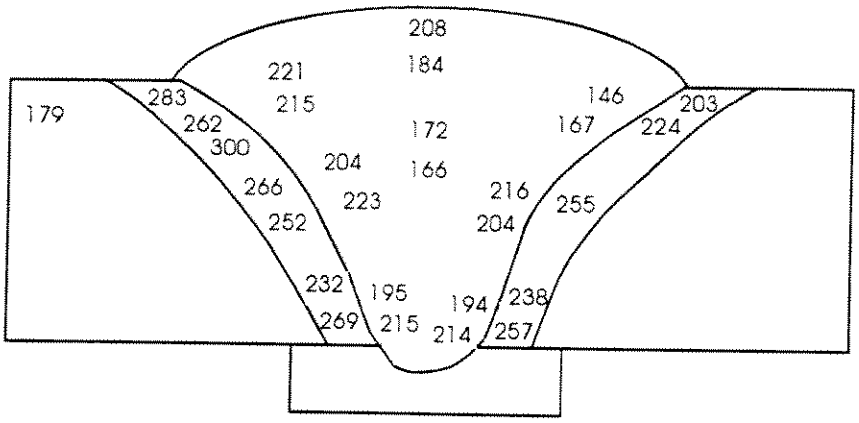

Hardness Test Data: Vickers 1 kg
Weld Identification: UL-8

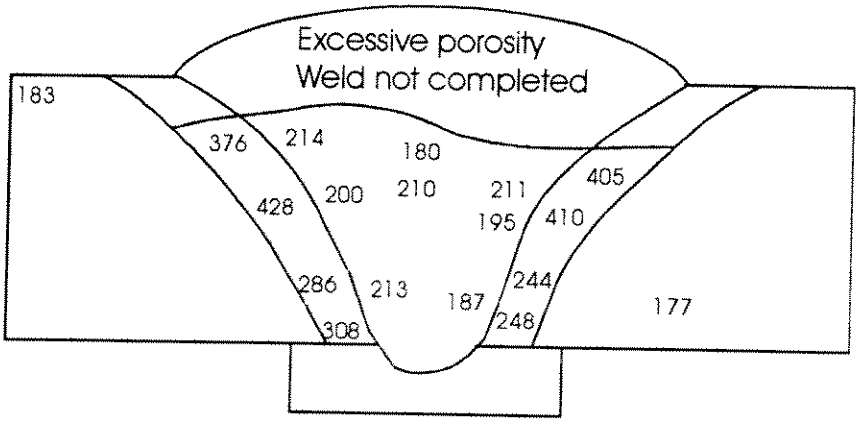

Hardness Test Data: Vickers 1 kg
Weld Identification: UL-9

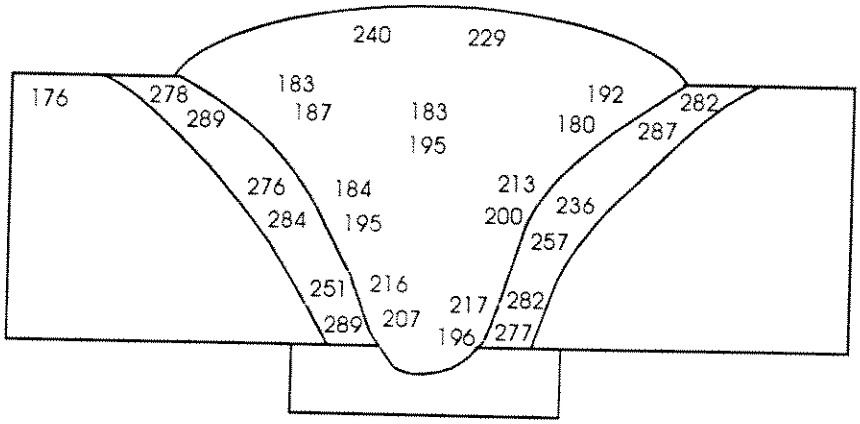

Hardness Test Data: Vickers 1 kg
Weld Identification: UL-10

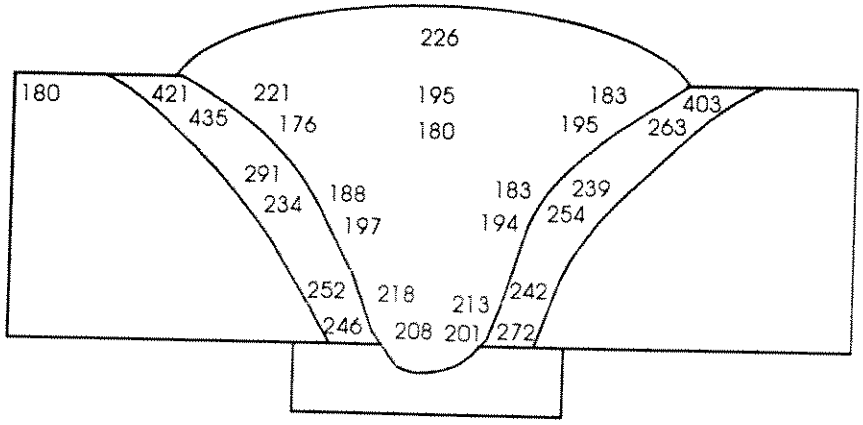

Hardness Test Data: Vickers 1 kg
Weld Identification: UL-11

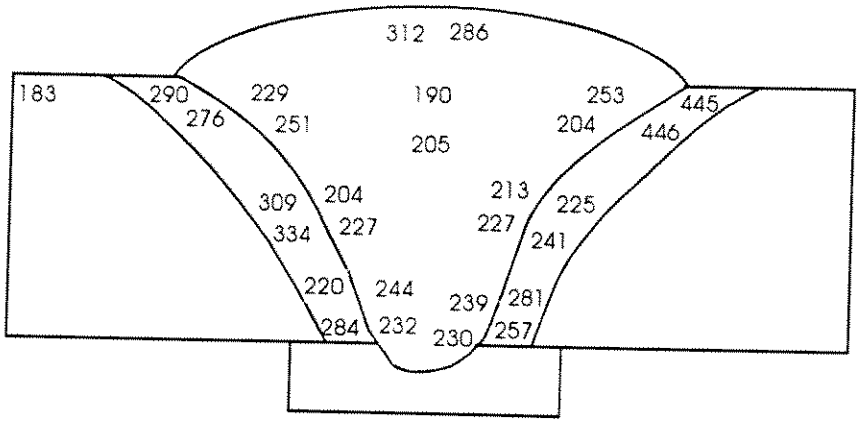

Hardness Test Data: Vickers 1 kg
Weld Identification: UL-12